Supplementary Information

Delocalized Solvation Structures Design Enables 600 Wh kg^{-1} Lithium Metal Pouch Cells

He Huang[1,2], Yitao Hu[3], Yajun Hou[4], Xingkai Wang[4], Qiujiang Dong[4], Zhixin Zhao[3], Mingfang Ji[4], Wanxing Zhang[4], Jinyang Li[4], Jianping Xie[1,2], Hao Guo[4,5]*, Xiaopeng Han[4]*, Xiaoping Ouyang[5]*, Wenbin Hu[1,4]*

[1]Joint School of National University of Singapore and Tianjin University, International Campus of Tianjin University, Binhai New City, Fuzhou 350207, China.

[2]Department of Chemical and Biomolecular Engineering, National University of Singapore, 4 Engineering Drive 4, Singapore 117585, Singapore.

[3]College of Intelligence and Computing, Tianjin University, Tianjin 300072, China.

[4]School of Materials Science and Engineering, Tianjin University, Tianjin 300072, China.

[5]State Key Laboratory of Advanced Chemical Power Sources, Zunyi, Guizhou 563003, China.

*Corresponding author. Email: guoh@tju.edu.cn; xphan@tju.edu.cn; oyxp2003@aliyun.com; wbhu@tju.edu.cn

Supplementary Discussions

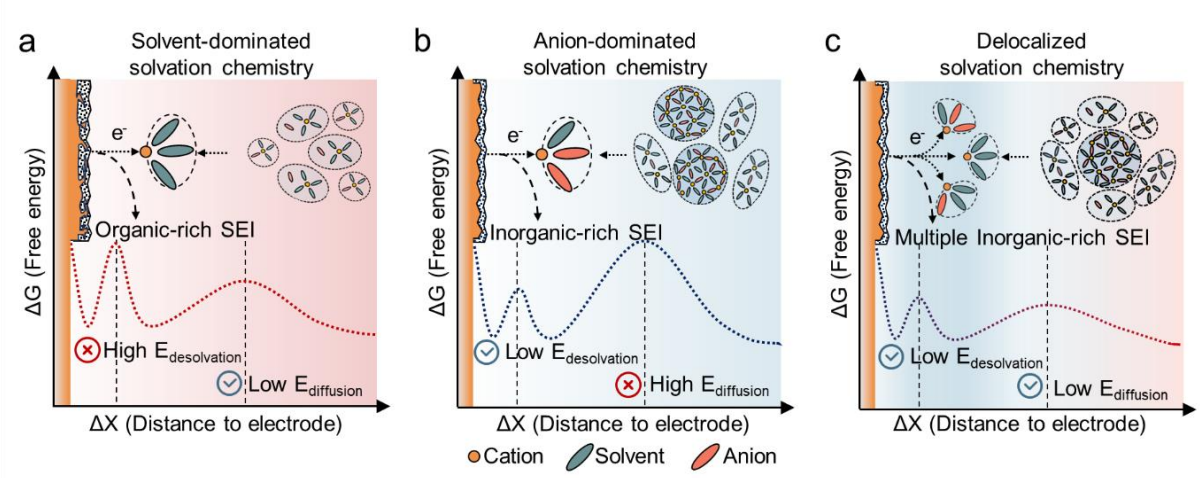

Supplementary Fig. 1|Schematic illustration of distinct solvation chemistries. a, Solvent-dominated solvation chemistry. **b,** Anion-dominated solvation chemistry. **c,** Delocalized solvation chemistry.

Supplementary Note 1

To further quantify the dispersion of the electrolyte microenvironment for different electrolytes, we simplify the solvation structure and introduce S_{config} into the electrolyte system, which can be expressed as:

$$S_{config} = \sum_{i=0}^{n} P_n S_{n-anions\ solvation\ structure} \quad (1)$$

$$S_{n-anions\ solvation\ structure} = -R \sum_{i=0}^{m} (X_n lnX_n + X_{m-n} lnX_{m-n}) \quad (2)$$

Where n is the number of anion sites in the solvation structure, P_n is the probability that the solvation structure with a specific number of anions, $S_{n\text{-}anions\ solvation\ structure}$ is the entropy of the solvation structure with a specific number of anions, R is the gas constant (8.314 J $mol^{-1}K^{-1}$), m is the number of anion or solvent sites in the solvation structure, X_n is the probability that different anions occupy a site, $X_{m\text{-}n}$ is the probability that different solvent molecules occupy a site. Notably, the variables P_n, X_n, and $X_{m\text{-}n}$ are greatly determined by the variety and abundance of lithium salts and solvents.

Despite rigorous screening to exclude solvents and salts with extreme $E_{solvation}$ or $E_{binding}$ values, significant P_n values persist in configurations involving single salts or solvents. Therefore, the semi-delocalized electrolyte (SDE) configuration of a single salt may not lead to a substantial increase in S_{config}. To facilitate calculation, we assume that both salts and solvents can equally occupy the four coordination sites, facilitating the quantification of solvation structures based on the available microstates. The UDE demonstrates significantly higher S_{config}, with 6.07×10^{-23} J K^{-1} for LE, 9.88×10^{-23} J K^{-1} for SDE, and 1.27×10^{-22} J K^{-1} for UDE. As the entropy contribution from these components increases, the coordination environments around Li^+ cations become more varied, leading to a wider array of solvation structures. This increased S_{config} disrupts dominant

solvation structures, fostering a more complex and stable electrolyte microenvironment, thereby achieving delocalized solvation structures.

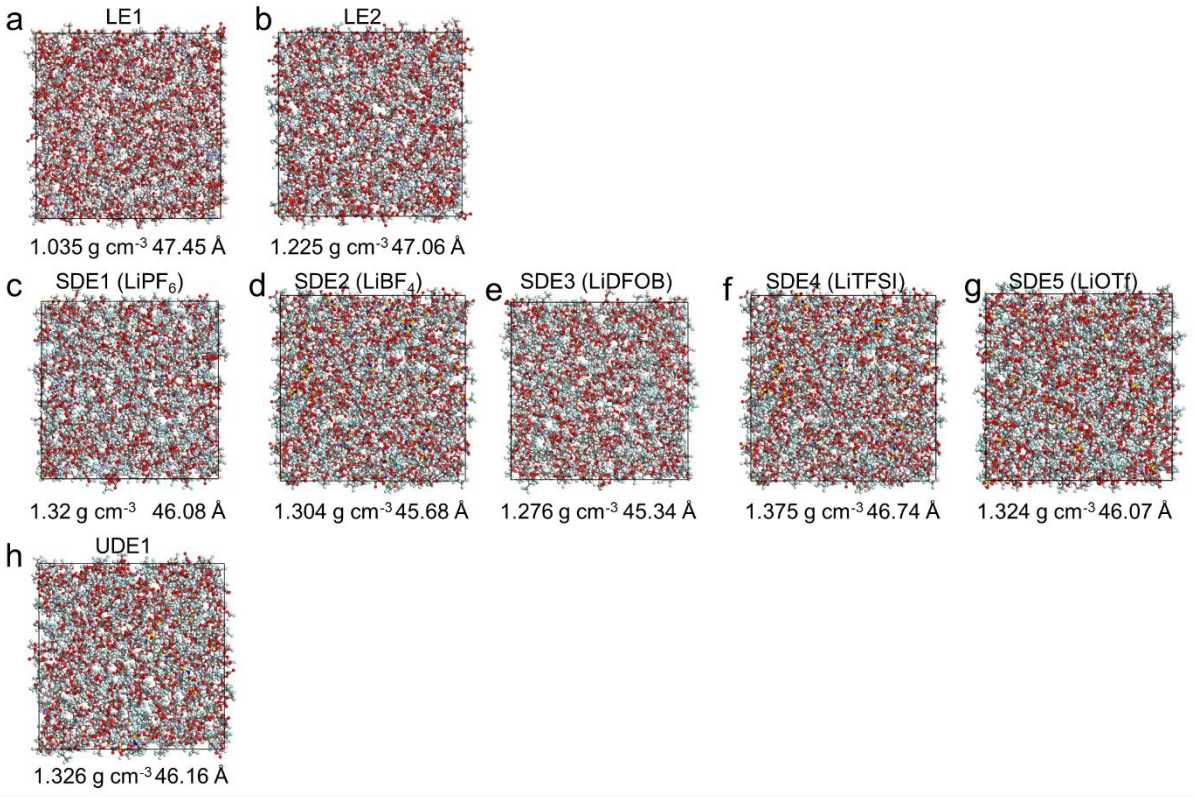

Supplementary Fig. 2|Molecular dynamics (MD) simulation models, correlation density, and simulated unit cell size of different electrolytes after 2ns of annealing. a, LE1. **b,** LE2. **c,** SDE1. **d,** SDE2. **e,** SDE3. **f,** SDE4. **g,** SDE5. **h,** UDE1. Note that all results are presented in the default style.

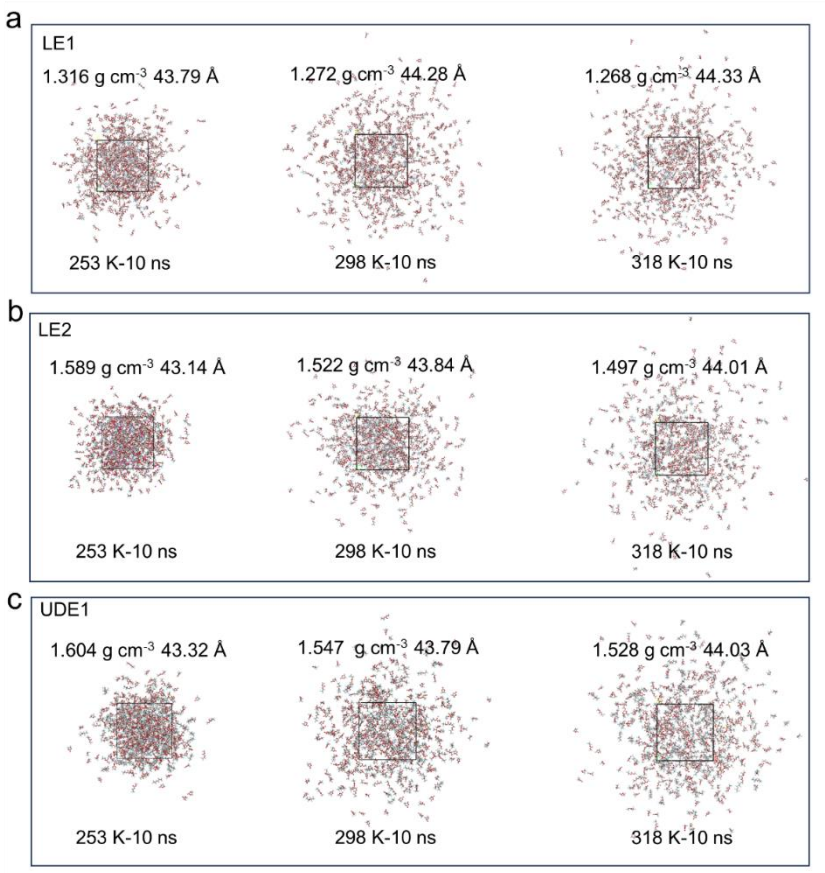

Supplementary Fig. 3|Molecular dynamics (MD) results after 2 ns of NPT simulations and 10 ns of NVT simulations for various LE and UDE electrolytes at different temperatures. a, LE1. **b,** LE2. **c,** UDE1. Note that all results are presented in the original style to reflect diffusion differences.

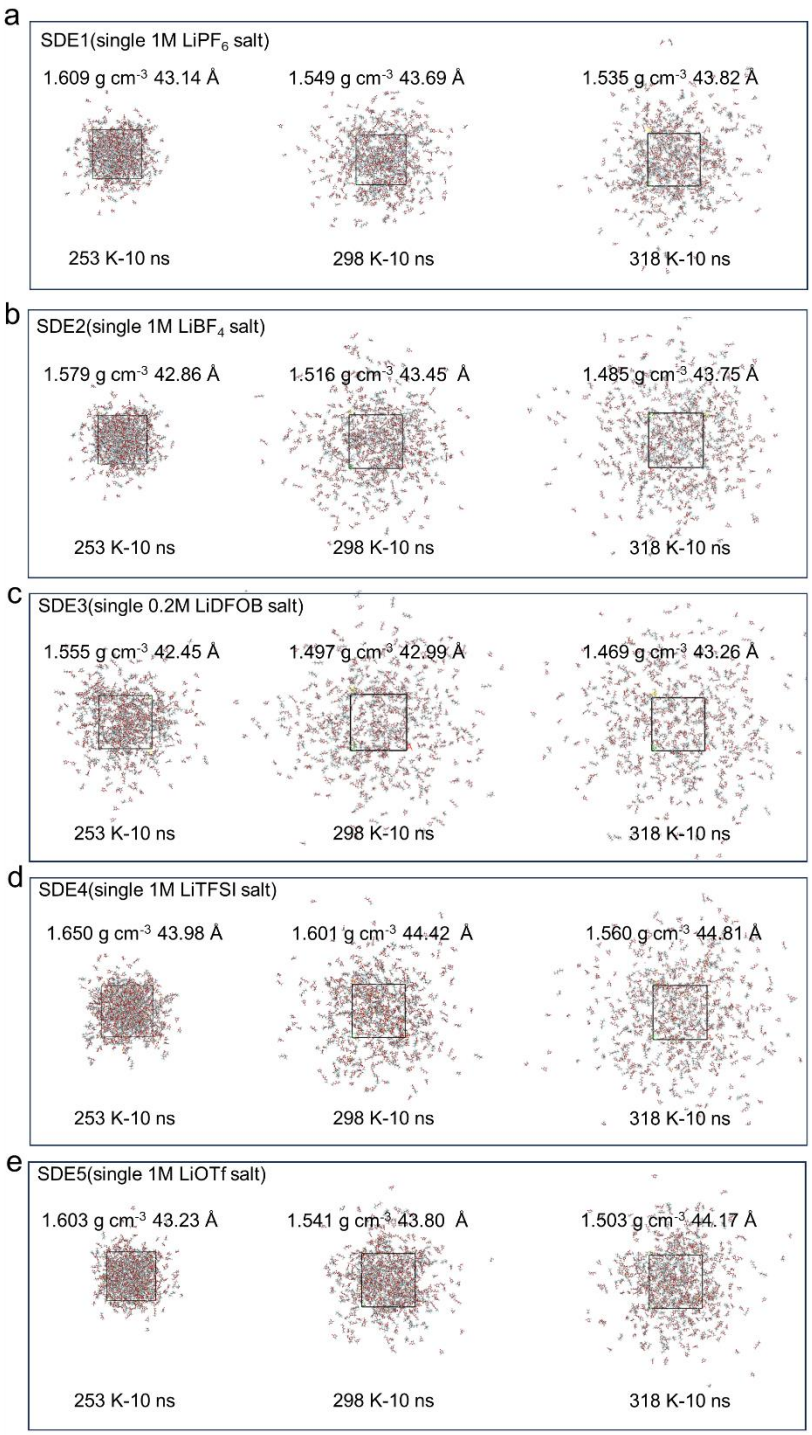

Supplementary Fig. 4|Molecular dynamics (MD) results after 2 ns of NPT simulations and 10 ns of NVT simulations for various SDE electrolytes at different temperatures. a, SDE1. **b,** SDE2. **c,** SDE3. **d,** SDE4. **e,** SDE5. Note that all results are presented in the original style to reflect diffusion differences.

Supplementary Note 2

The LE1 electrolyte displays a prominent solvent-dominated peak in the higher coordination region, while LE2, despite being similarly solvent-dominated, lacks this peak, indicating a more constrained coordination environment (Supplementary Fig. 5). The series SDE electrolytes demonstrate more intricate solvation profiles, incorporating contributions from both solvents and anions (Supplementary Fig. 6). Specifically, the SDE1, SDE2 and SDE5 electrolytes exhibit pronounced Li-anion associations in regions of lower coordination, whereas SDE3 and SDE4 display a higher proportion of interactions in the high coordination regime. Although the semi-delocalized electrolytes broaden the solvation structure to some degree, they remain significantly influenced by the presence of a single lithium salt, resulting in a noticeable solvation structural tropism. In contrast, UDE1 reveals a broader Li-anion distribution, suggesting more complex and diverse solvation structures.

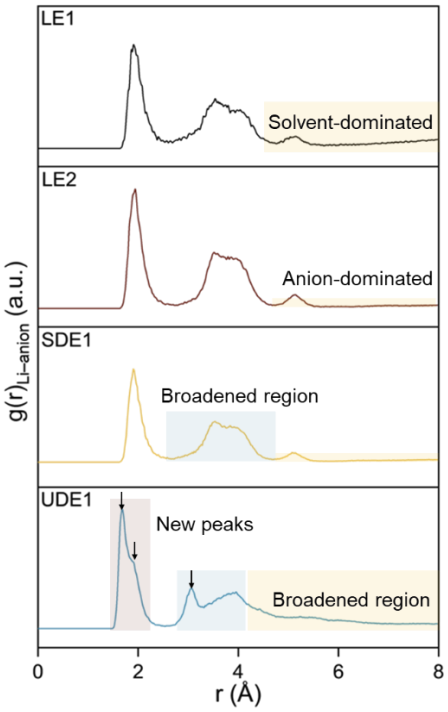

Supplementary Fig. 5|The radial distribution function (RDF) plots of Li–anion in LE1, LE2, SDE1, and UDE1 electrolytes.

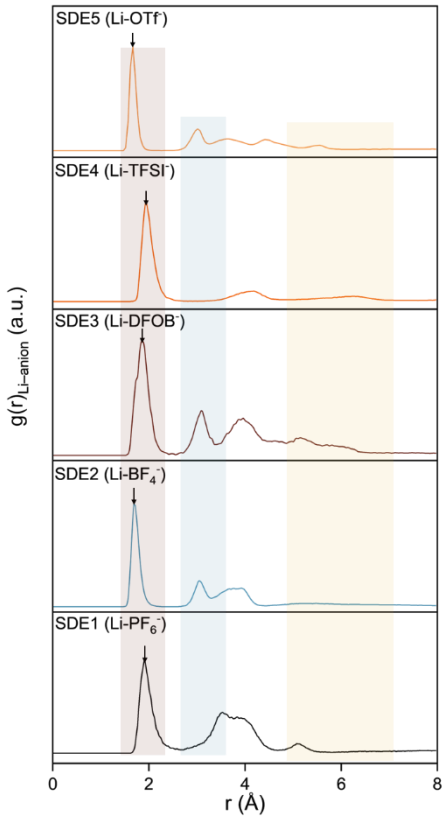

Supplementary Fig. 6|The radial distribution function (RDF) plots of Li-anion in different SDE electrolytes.

Supplementary Note 3

The Raman spectra illustrate the relative intensity of Li-anion and Li-solvent interactions across different electrolyte systems (UDE1, UDE2, SDE1, and LE1) (Supplementary Fig. 7). The red dashed curve represents the fraction of Li-anion interactions, while the blue dashed curve denotes the fraction of Li-solvent interactions. LE1 predominantly displays a solvent-coordinated Li-ion structure, suggesting a limited interaction between Li and anions. Conversely, LE2 reveals a substantial increase in Li-anion interactions, underscoring a different delocalized solvation environment. As delocalization increases, both SDE1 and UDE1 demonstrate broader and more complex solvation structures, with UDE1 showcasing a particularly intricate and diverse solvation microenvironment, indicative of a more balanced interplay between Li-anion and Li-solvent interactions.

The Li^+ solvation environments of various electrolytes are reflected in their chemical shifts, with notable variations attributable to differing degrees of delocalization (Supplementary Fig. 8 and 9). These differences influence the extent of lithium-ion shielding, underscoring the distinct solvation structures present in each electrolyte. Furthermore, it can be revealed that the solvation environment of the electrolyte is strongly impacted by the specific lithium salts used, highlighting that the SDE design hardly achieves complete delocalization of the solvation microenvironment.

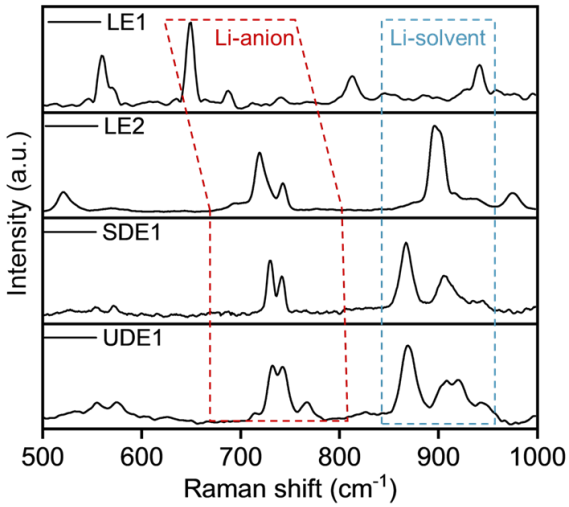

Supplementary Fig. 7|Raman spectra of various electrolytes.

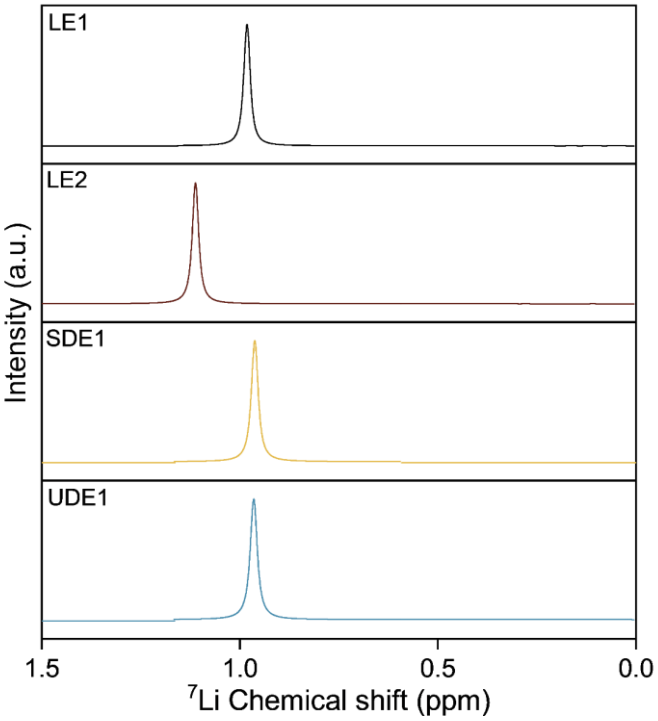

Supplementary Fig. 8|^{7}Li nuclear magnetic resonance (NMR) spectra of LE1, LE2, SDE1, and UDE1 electrolytes.

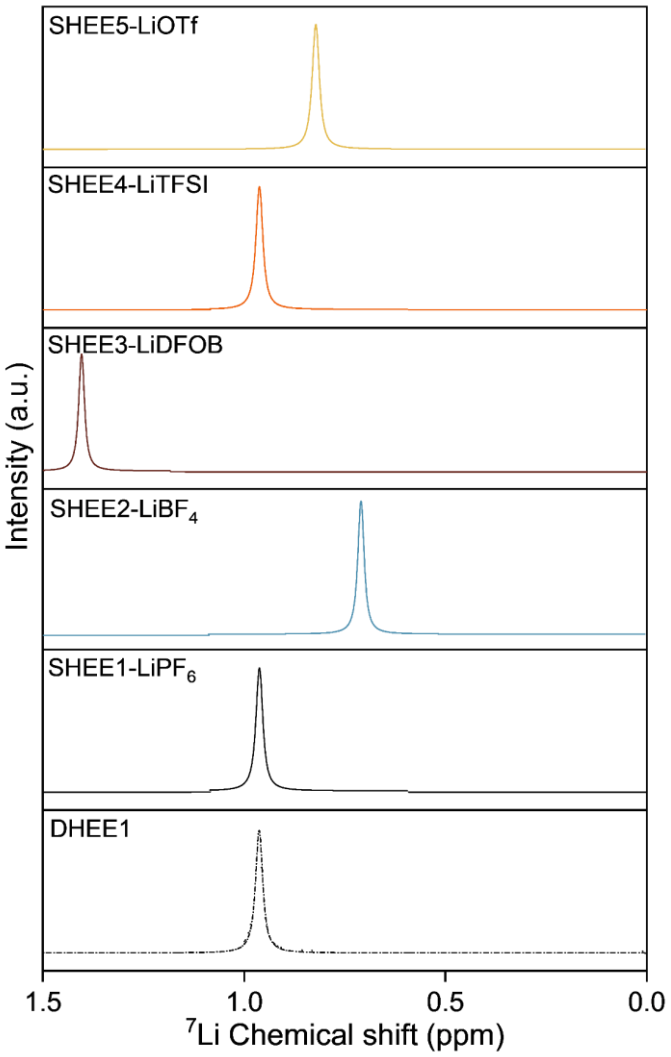

Supplementary Fig. 9|^{7}Li NMR spectra of LE1, LE2, SDE1, and UDE1 electrolytes.

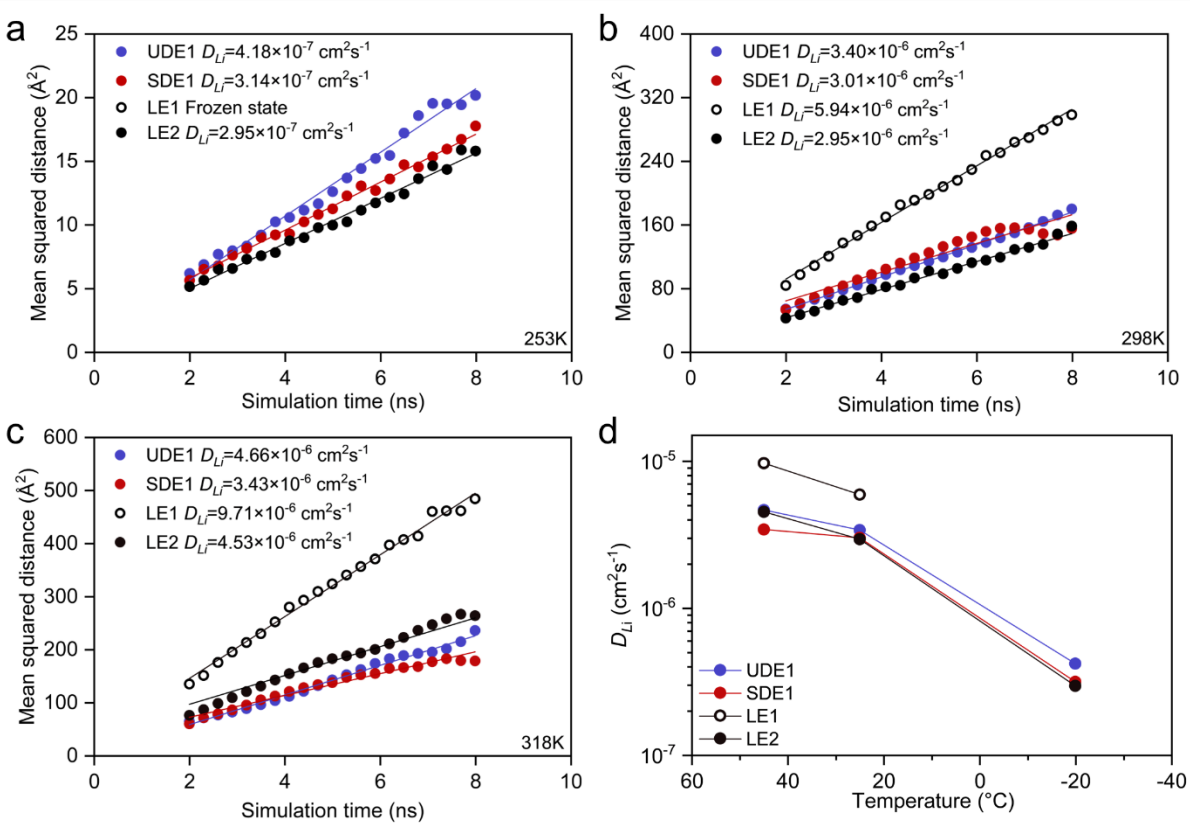

Supplementary Fig. 10|The lithium-ion self-diffusion coefficient (D_{Li}) from the MD simulated mean squared displacement (2 ns to 8 ns) for LE1, LE2, SDE1, and UDE1 electrolytes at different temperatures. a, 253K result. **b,** 298K result. **c,** 318K result. **d,** D_{Li} of different electrolytes from 45°C to -20°C.

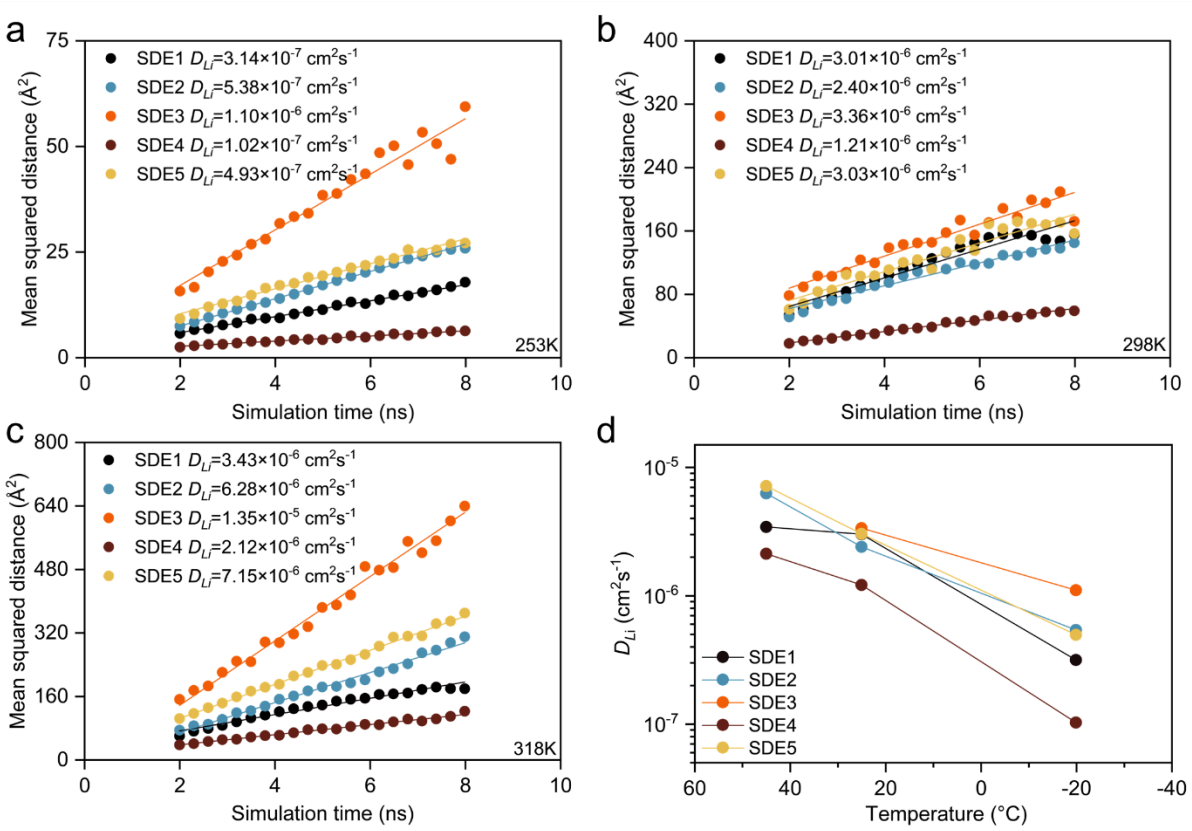

Supplementary Fig. 11|The lithium-ion self-diffusion coefficient (D_{Li}) from the MD simulated mean squared displacement (2 ns to 8 ns) for SDE series electrolytes at different temperatures. a, 253K result. **b,** 298K result. **c,** 318K result. **d,** D_{Li} of different electrolytes from 45°C to -20°C.

Supplementary Note 4

To identify the interphase and Li^+ diffusion difference, the DRT test was conducted in NCM811||Li coin cells with different electrolytes after 50 cycles (Supplementary Fig. 12). The τ of Li+ crossing interphases falls between 10^{-5} to 10^{-2} s, and that of Li^+ diffusion falls between 10 to 100 s. The UDE1 electrolyte exhibits low $R_{interphase}$ and $R_{diffusion}$, indicating that delocalized solvation structures derived by UDE electrolyte can simultaneously achieve low Li^+ desolvation energy and high Li^+ diffusion rate.

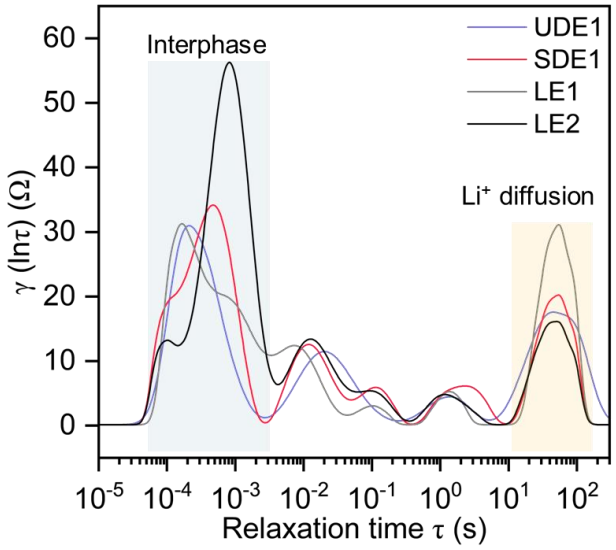

Supplementary Fig. 12|Distribution of Relaxation Times (DRT) results of NCM811||Li coin cells with different electrolytes after 50 cycles.

Supplementary Note 5

To evaluate the screening strategy and electrolyte design for UDE electrolytes, different electrolytes were prepared to test the suitability with high-voltage cathode and Li metal anode in coin cells. Notably, capacity retention of Cathode||Li cion cells increases in the order of LE1 to LE2 to SDE1 to UDE1, where UDE1 electrolyte delivers a much higher discharge capacity retention (86.2% for 4.3 V-Ni90, 90.8% for 4.45 V-NCM811, and 89% for 4.6 V-LCO, respectively) after 200 cycles at 1C (1C = 200 mAh g^{-1}) (Supplementary Figs. 13 and 14). Similarly, the Cu||Li with UDE1 electrolyte exhibits stable lithium metal plating/stripping voltage profiles with high Coulombic efficiency above 97.7% and low polarization after 100 cycles, whereas that of LE1 only remains at 4.0% (Supplementary Fig. 15). The remarkable improvement is correlated with solvation structure diversity, also demonstrating strong consistency with the Linear Sweep Voltammetry (LSV) results (Supplementary Fig. 16). The screened electrolytes (LE2, SDE1, and UDE1) demonstrated significantly enhanced high-voltage stability, whereas LE1 exhibited pronounced oxidative decomposition.

Furthermore, we evaluated the performance of the SDE electrolyte series (SDE1-SDE5, details in Supplementary Table 3). Notably, performance fluctuations were observed within this series (Supplementary Figs. 17–19). These variations can be attributed to the single-salt configuration in the SDE electrolytes, which inherently restricts the extent of delocalization achievable in this electrolyte system. This limitation in delocalization likely impacts the stability and overall effectiveness of ion transport within the series.

To rigorously assess the general applicability of the UDE design, we conducted a systematic evaluation of a series of UDE electrolytes (UDE1-UDE3; detailed in Supplementary Table 3). These electrolytes consistently demonstrated stable electrochemical performance across multiple parameters (Supplementary Figs. 20-22), underscoring the robustness and adaptability of the delocalized UDE configuration. Such findings substantiate the validity of this design strategy, confirming its potential to enhance electrochemical stability and broaden its applicability within advanced battery systems.

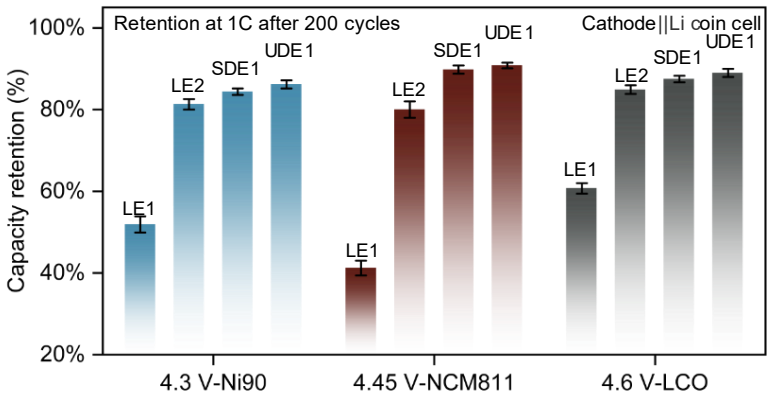

Supplementary Fig. 13|The capacity retentions of 4.3 V Ni90||Li, 4.45 V NCM811||Li, and 4.6 V LCO||Li coin cells in the electrolytes of LE1, LE2, SDE1, and UDE1 after 200 cycles at 1C.

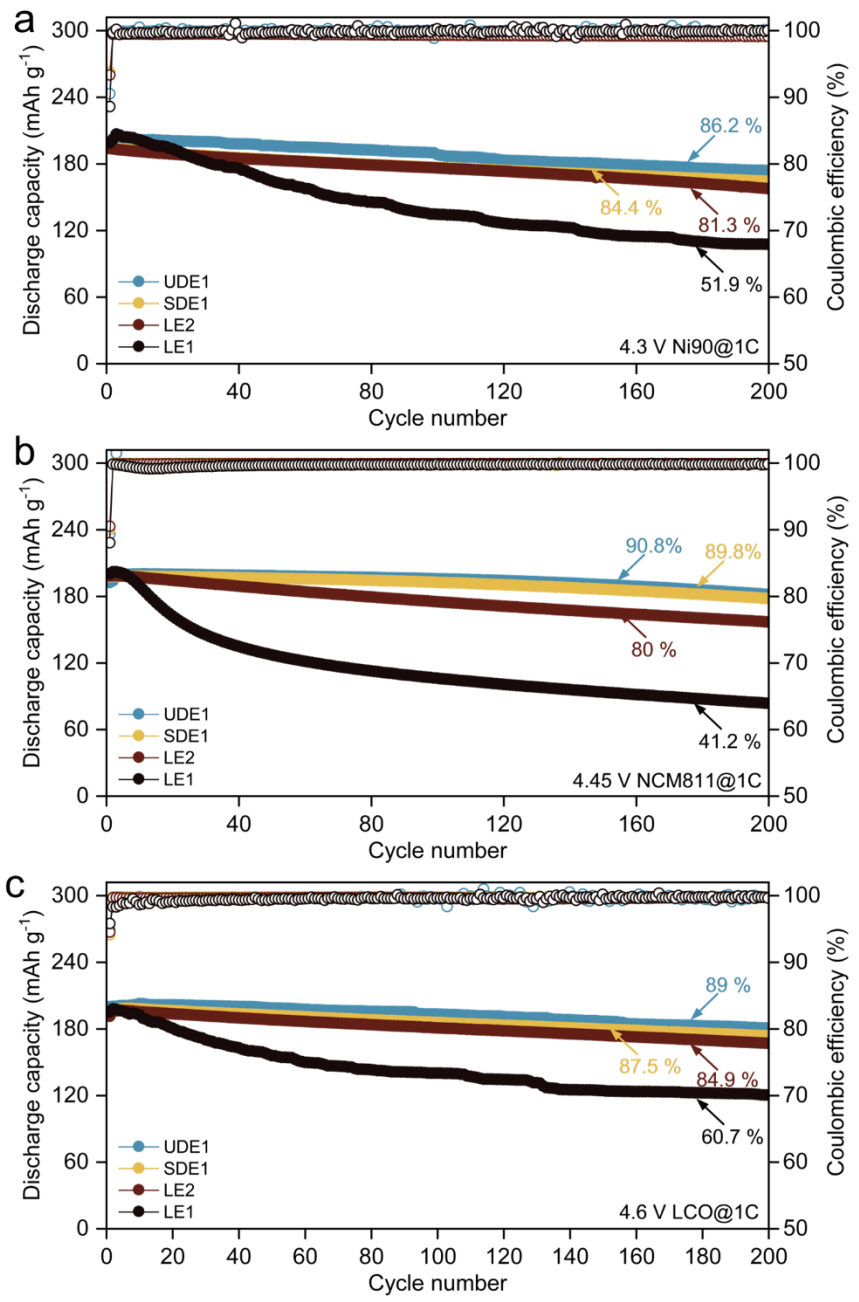

.

Supplementary Fig. 14|Cycling performance of different high-voltage cathode||Li coin cells with different electrolytes at 1 C charge/discharge. a, 4.3 V Ni90||Li coin cells. **b,** 4.45 V NCM811||Li coin cells. **c,** 4.6 V LCO||Li coin cells.

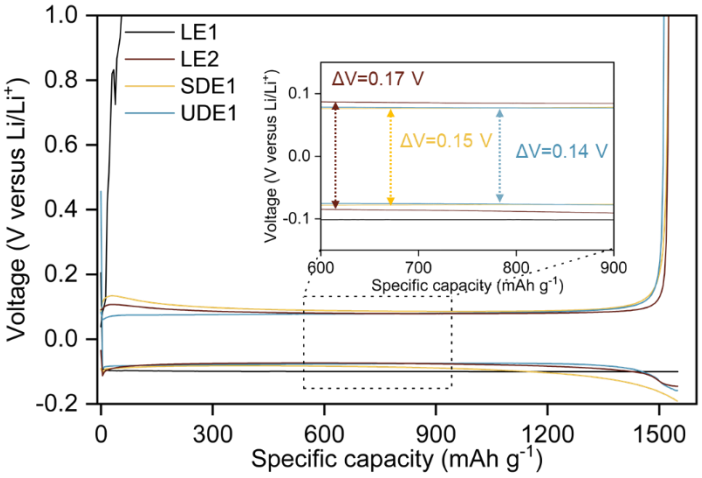

Supplementary Fig. 15|Li-metal plating/stripping profiles on a Cu working electrode cycled in LE1, SDE1, and UDE1 electrolytes at a current density of 1 mA cm^{-2} after 100 cycles.

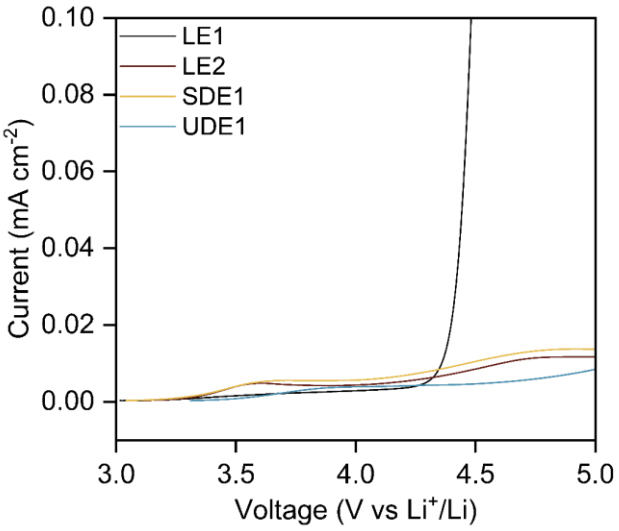

Supplementary Fig. 16|Positive liner sweep voltammograms (LSV) sweep to gauge the oxidation stabilities of the LE1, LE2, SDE1, and UDE1 electrolytes as evaluated on stainless steel||Li cells for different electrolytes at a scan rate of 0.1 mV s^{-1}.

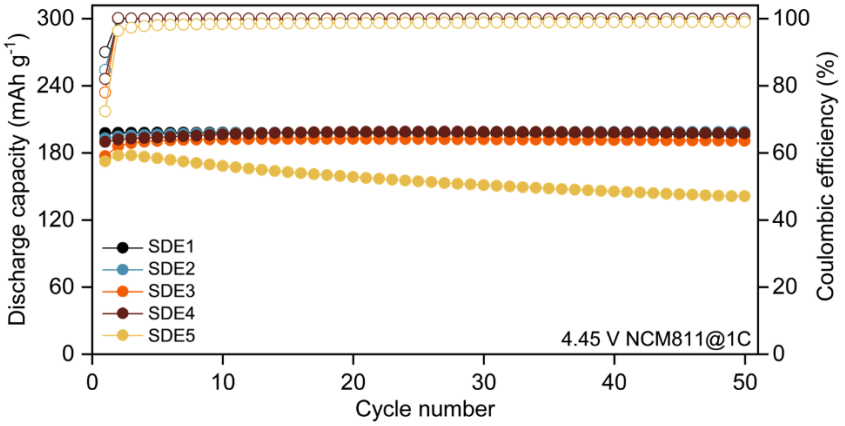

Supplementary Fig. 17|Cycling performance of 4.45 V NCM811||Li coin cells with SDE1, SDE2, SDE3, SDE4, and SDE5 electrolytes at 1 C charge/discharge.

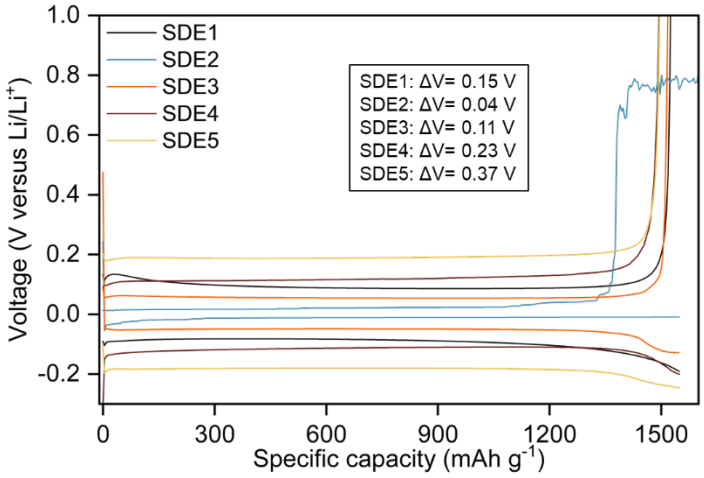

Supplementary Fig. 18|Li-metal plating/stripping profiles on a Cu working electrode cycled in SDE1, SDE2, SDE3, SDE4, and SDE5 electrolytes at a current density of 1 mA cm^{-2} after 100 cycles.

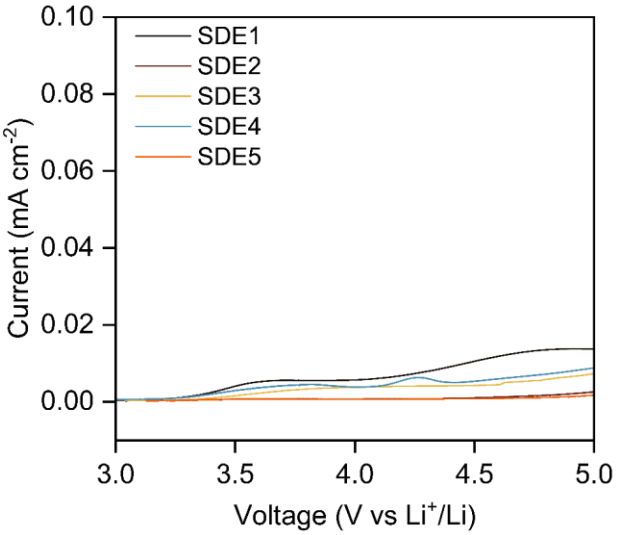

Supplementary Fig. 19|Positive liner sweep voltammograms (LSV) sweep to gauge the oxidation stabilities of the SDE1, SDE2, SDE3, SDE4, and SDE5 electrolytes as evaluated on stainless steel||Li cells for different electrolytes at a scan rate of 0.1 mV s^{-1}.

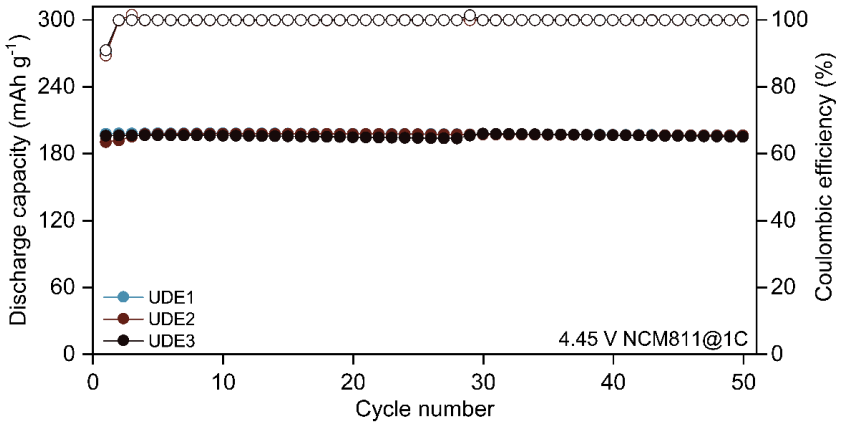

Supplementary Fig. 20|Cycling performance of 4.45 V NCM811||Li coin cells with UDE1, UDE2, and UDE3 electrolytes at 1 C charge/discharge.

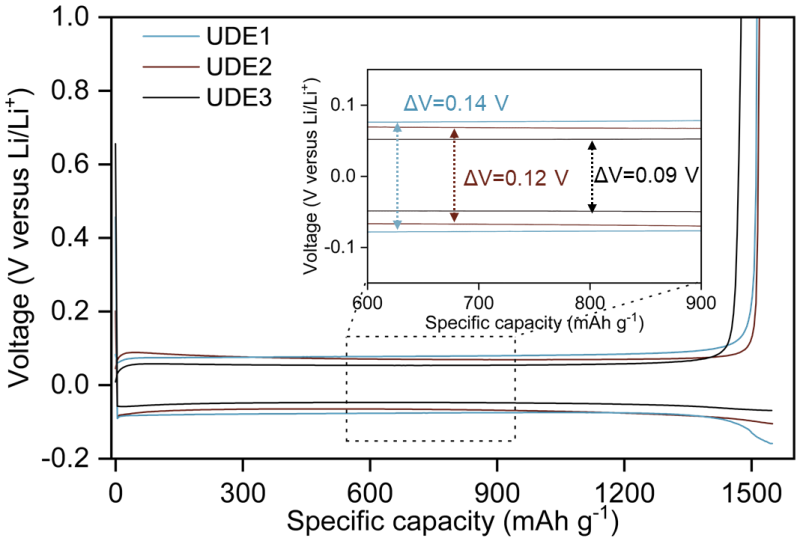

Supplementary Fig. 21|Li-metal plating/stripping profiles on a Cu working electrode cycled in UDE1, UDE2, and UDE3 electrolytes at a current density of 1 mA cm^{-2} after 100 cycles.

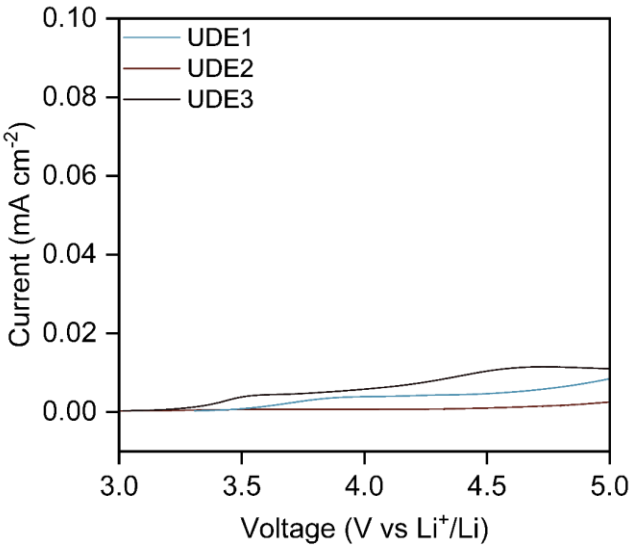

Supplementary Fig. 22|Positive liner sweep voltammograms (LSV) sweep to gauge the oxidation stabilities of the UDE1, UDE2, and UDE3 electrolytes as evaluated on stainless steel||Li cells for different electrolytes at a scan rate of 0.1 mV s^{-1}.

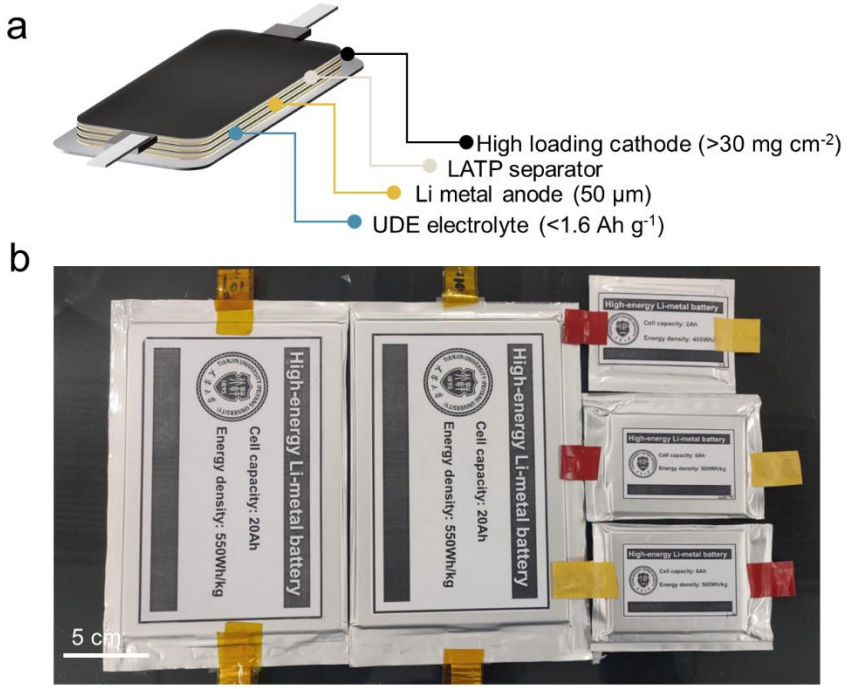

Supplementary Fig. 23|Schematic illustration of high-energy lithium metal pouch cells. a, Schematic depiction of the assembly process for lithium metal pouch cells. **b,** Physical representation of the fully assembled pouch cells.

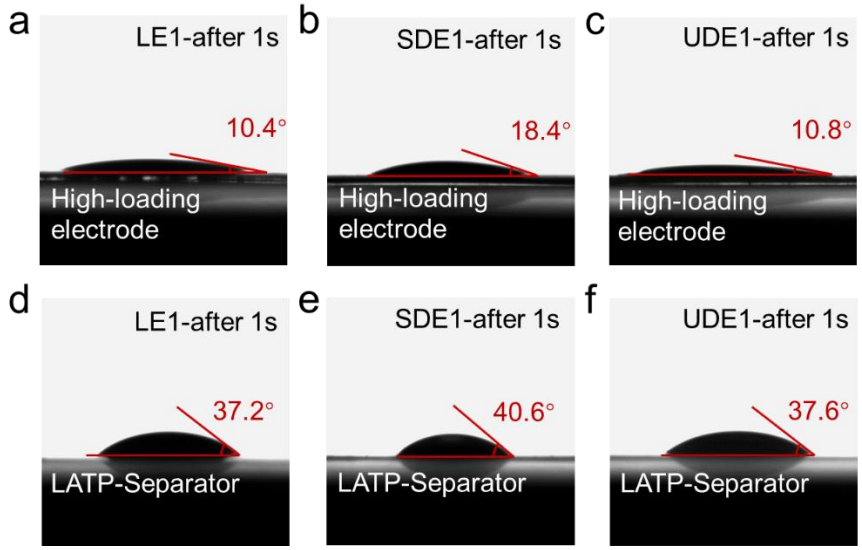

Supplementary Fig. 24|Wettability test for various electrolytes. a-c, Contact angle measurements for LE1 (**a**), LE2 (**b**), and UDE1 (**c**) electrolytes on a high-loading electrode after 1 second. **d-f,** Contact angle measurements for LE1 (**d**), LE2 (**e**), and UDE1 (**f**) electrolytes on a LATP separator after 1 second.

Supplementary Note 6

In the Battery500 performance evaluation, we tested a range of cathode materials and capacities to rigorously assess the potential of our electrolyte design across different configurations (Supplementary Figs. 25-28, and details in Supplementary Tables 7-10). Despite the aggressive battery configuration, an initial specific energy density of 510.1 Wh kg^{-1} was achieved in a 1.9 Ah $LiNi_{0.8}Co_{0.1}Mn_{0.1}O_2$ (NCM811)||Li pouch cell, considering the mass of all components within the pouch cells (Supplementary Figs. 25). The NCM811||Li pouch cell with UDE1 electrolyte exhibited stable cycling performance, retaining 404.1 Wh kg^{-1} after 150 cycles, with no notable capacity drop even after 300 cycles. In contrast, cells utilizing LE1 and SDE1 electrolytes exhibited rapid polarization and precipitous capacity drops after just 20 and 83 cycles, respectively. This capacity degradation was further exacerbated under elevated charging voltage, as evidenced by the 1.8 Ah $LiCoO_2$ (LCO)||Li pouch cell (Supplementary Figs. 26), where the LE1-based and SDE1-based pouch cells displayed a pronounced capacity drop after only 12 cycles and 32 cycles, respectively. Only the delocalized UDE1 electrolyte delivered superior high-voltage performance, preserving 85.2% of the initial capacity from 519.3 Wh kg^{-1} to 442.6 Wh kg^{-1} after 100 cycles. To further enhance the practical energy density of LMBs, we adopted aggressive design parameters for 6.9 Ah and 23.2 Ah NCM811||Li pouch cells (Supplementary Figs. 27 and 28), achieving high energy density and stable cycling of 555.1 Wh $kg^{-1}$and 565.8 Wh kg^{-1}, respectively.

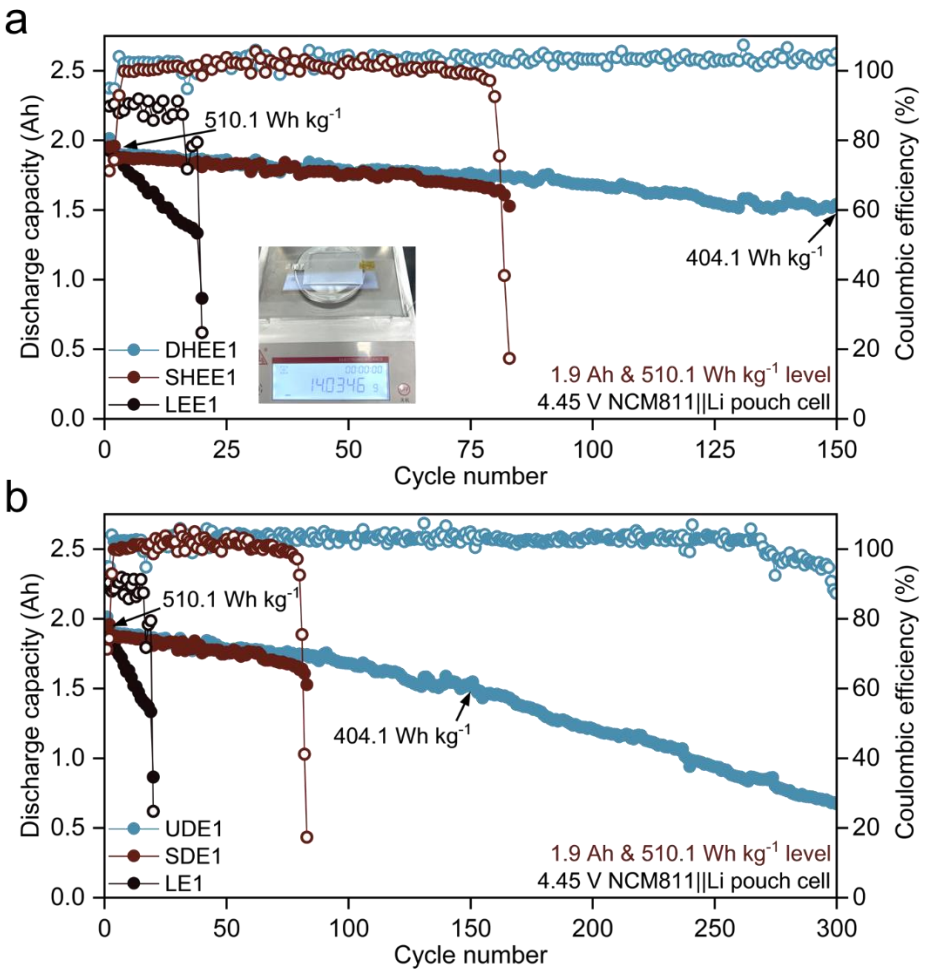

Supplementary Fig. 25|Cycling performance of 1.9 Ah 4.45 V-NCM811||Li pouch cells with different electrolytes at 0.1 C charge/0.5C discharge in the range 3-4.45 V after one formation cycle at 0.1 C charge/discharge in the range 3-4.45 V after 150 cycles (a). after 300 cycles without a capacity drop (b).

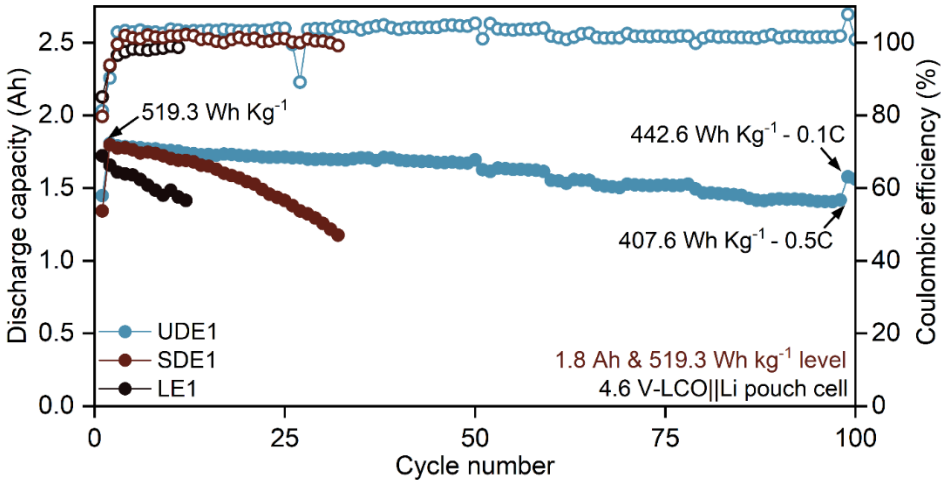

Supplementary Fig. 26|Cycling performance of 1.8 Ah 4.6 V-LCO||Li pouch cells with different electrolytes at 0.1C charge/0.5C (or 0.1C) discharge in the range 3-4.6 V after one formation cycle at 0.1C charge/discharge in the range 3-4.45 V.

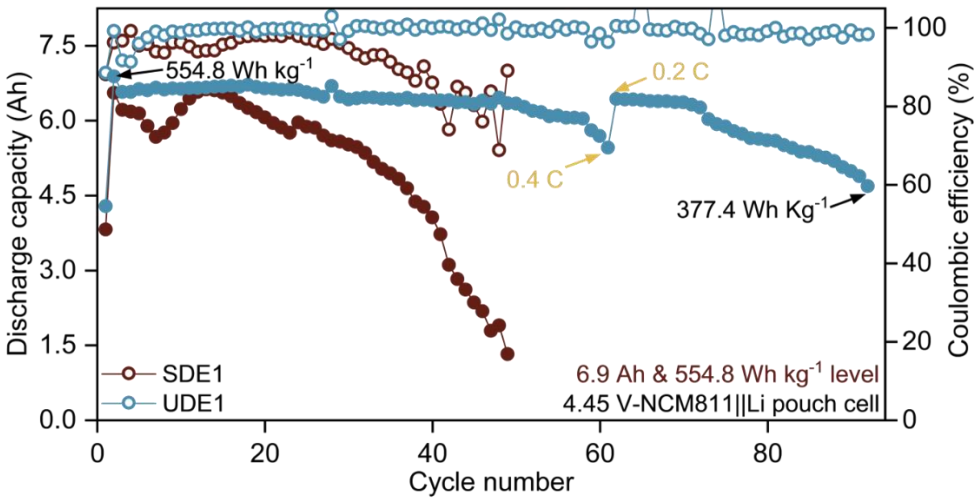

Supplementary Fig. 27|Cycling performance of 6.9 Ah 4.45 V-NCM811||Li pouch cells with different electrolytes at 0.1C charge/0.4C (or 0.2C) discharge in the range 2.9-4.45 V after one formation cycle at 0.1 C charge/discharge in the range 2.9-4.0 V.

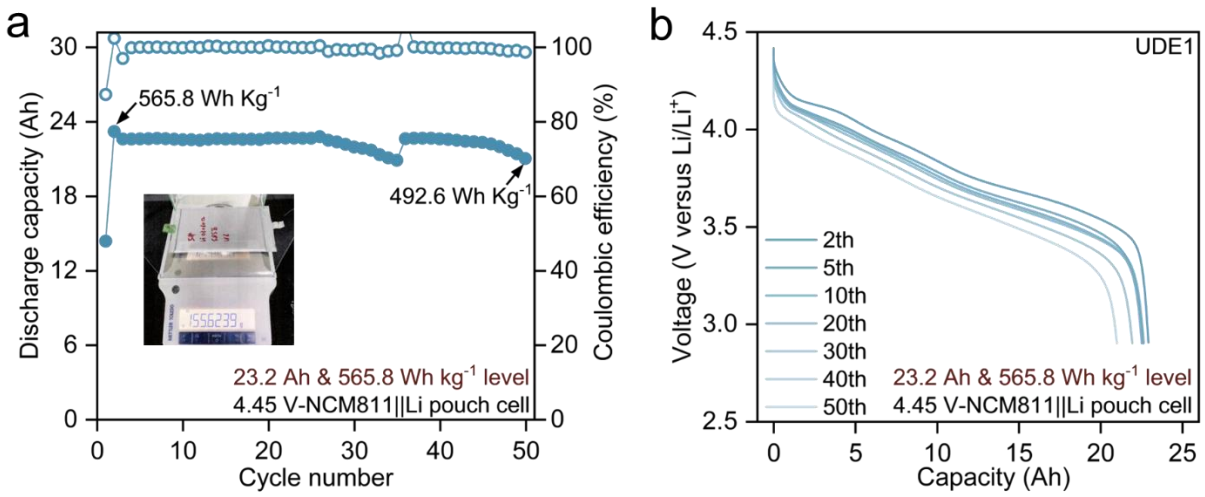

Supplementary Fig. 28|Cycling performance of 23.2 Ah 4.45 V-NCM811||Li pouch cells with UDE1 electrolytes at 0.1C charge/0.4C (or 0.2C) discharge in the range 2.9-4.45 V after one formation cycle at 0.1 C charge/discharge in the range 2.9-4.0 V (a), and the corresponding discharge capacity-voltage profiles at different cycles (b).

Supplementary Fig. 29|The digital photograph of the burnt-out Li-metal pouch cell with traditional LE1 electrolyte during the cycling.

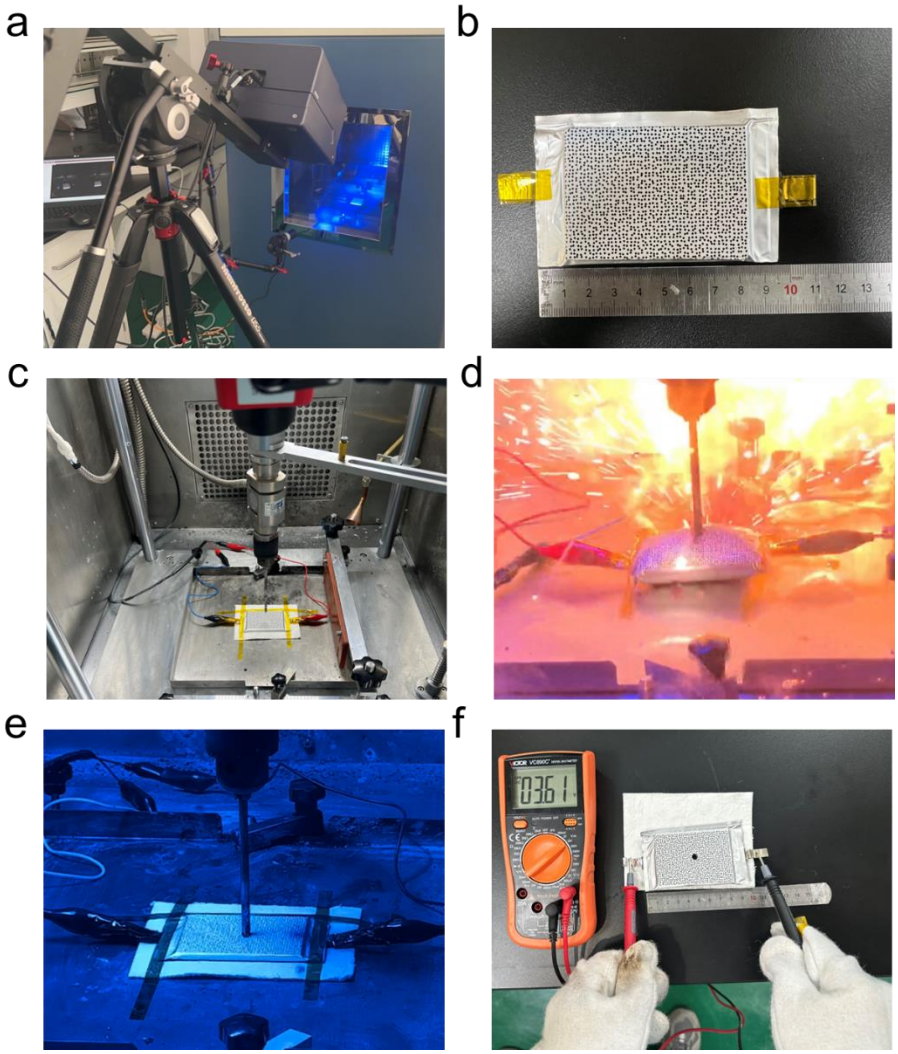

Supplementary Fig. 30|The nail-penetration tests for 6.9 Ah NCM811||Li pouch cells. a, The strain and temperature mapping system. **b,** The NCM811||Li pouch cell with strain monitoring points. **c,** The nail-penetration test equipment. **d,** The NCM811||Li pouch battery with LE1 electrolyte exploded during the nail penetration test. **f,** The NCM811||Li pouch battery with LE1 electrolyte exploded during the nail penetration test. **e,** The NCM811||Li pouch battery with UDE1 electrolyte unexploded during the nail penetration test. **f,** Post-nail penetration voltage measurement for NCM811||Li pouch cell with UDE1 electrolyte.

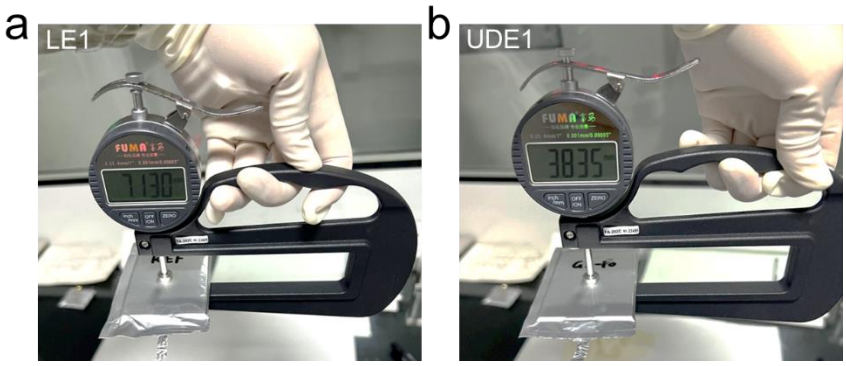

Supplementary Fig. 31|The thickness comparison of 6.9 Ah NCM811||Li pouch cells pouch using different electrolytes after one formation cycle. a, LE1 electrolyte. **b,** UDE1 electrolyte.

Supplementary Note 7

In the UDE design, perfluorinated components were strategically incorporated to confer broad thermal adaptability, effectively addressing the risks of combustion and freezing during real-world cycling conditions (Supplementary Fig. 31). This modification enhances the electrolyte's thermal resilience, ensuring safer operation across a wide temperature range. Furthermore, surface temperature monitoring conducted throughout the cycling of a 6.9 Ah NCM811||Li pouch cell containing the UDE1 electrolyte demonstrated remarkably stable thermal behavior, with minimal temperature fluctuations observed (Supplementary Fig. 32). This stability underscores the superior thermal management provided by the delocalized solvation structure in the UDE electrolyte, supporting its suitability for high-performance applications under demanding environmental conditions.

To further validate the stability and safety of the Li-metal pouch cell, we conducted an over-discharge assessment of 7 Ah Ni90||Li pouch cells, utilizing the UDE1 electrolyte over a series of charge-discharge cycles. The UDE1-based pouch cell demonstrated an exceptionally high energy density of 776.2 Wh kg^{-1} when discharged to 1.5 V, maintaining stable cycling performance beyond 10 cycles (Supplementary Fig. 33). These results emphasize the robust safety performance of the UDE1 electrolyte, demonstrating its capability to support high-energy-density LMBs.

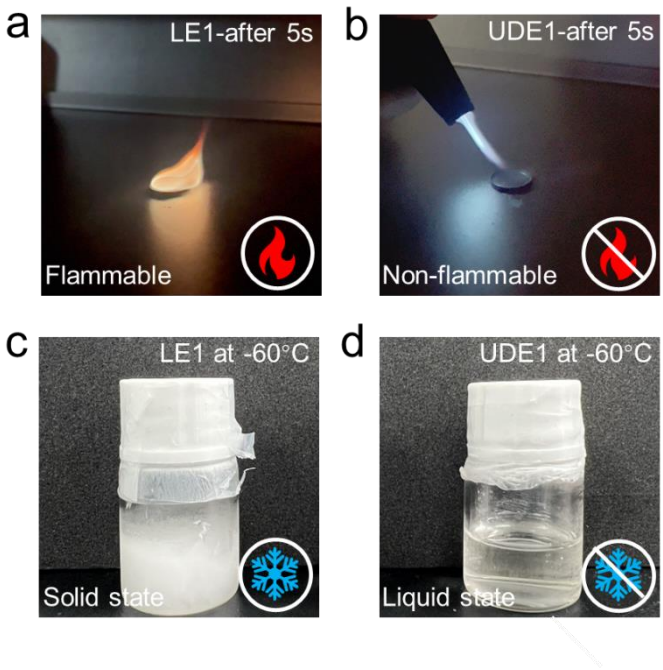

Supplementary Fig. 32|The fire and freeze resistance tests. a, The fire resistance test for LE1 electrolyte. **b,** The fire resistance test for UDE1 electrolyte. **c,** The freeze resistance test for LE1 electrolyte. **d,** The freeze resistance test for UDE1 electrolyte.

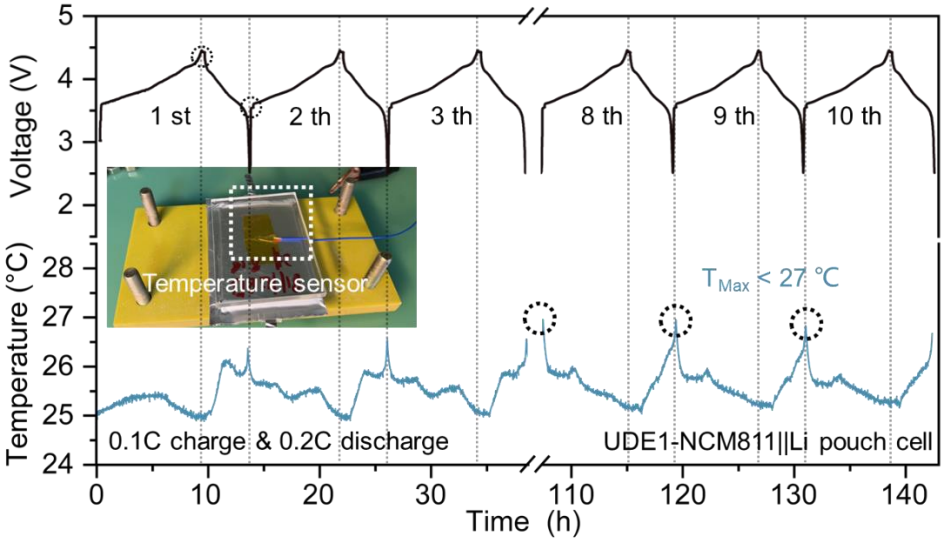

Supplementary Fig. 33|Voltage profiles and corresponding temperature change curves for the 6.9 Ah 4.45 V-NCM811||Li battery with UDE1 electrolyte during the first 10 cycles.

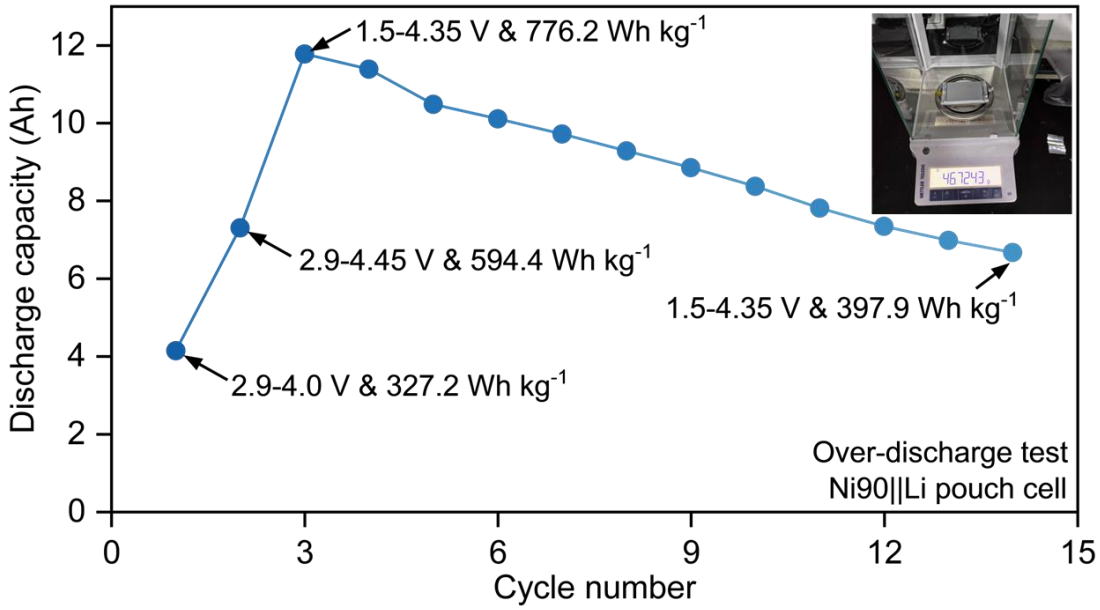

Supplementary Fig. 34|The Over-discharge test for 7 Ah Ni90||Li pouch cells.

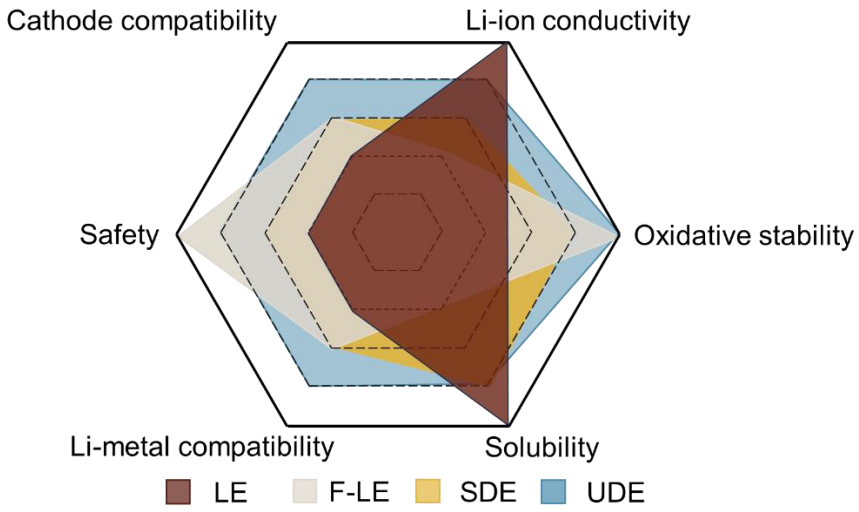

Supplementary Fig. 35|Performance metrics comparison of different electrolytes.

Supplementary Note 8

In-situ optical microscopy was conducted to observe the Li plating and stripping behavior in different electrolytes, as shown in Supplementary Fig. 35. In the LE-Li electrode, the initial lithium plating is characterized by pronounced dendritic growth, followed by substantial dead lithium formation after the first stripping cycle. This non-uniform deposition persists throughout subsequent cycles, culminating in a significant accumulation of dead lithium by the fifth cycle, indicative of poor electrochemical stability and reduced cycling efficiency. In contrast, the UDE-Li electrolyte exhibits a highly uniform lithium deposition from the first plating cycle, with negligible dead lithium formation post-stripping. This homogeneity is maintained through the fifth cycle, underscoring the electrolyte's superior electrochemical stability and enhanced interfacial ion transport.

Furthermore, we conducted TEM imaging to investigate the microstructural characteristics of lithium deposits formed on the Cu grid in different electrolytes (Supplementary Fig. 36). In the case of the LE1 electrolyte, the pronounced formation of lithium dendrites is observed, accompanied by the development of a thick, organic-rich SEI layer. In the case of the LE1 electrolyte, the pronounced formation of lithium dendrites is observed, accompanied by the development of a thick, organic-rich SEI layer. In contrast, the UDE1 electrolyte promotes a more compact and uniform lithium deposition, with a significantly thinner SEI that is predominantly inorganic-rich. This thinner, inorganic SEI enhances structural stability, facilitating smoother and more continuous lithium plating, and effectively mitigating dendrite growth.

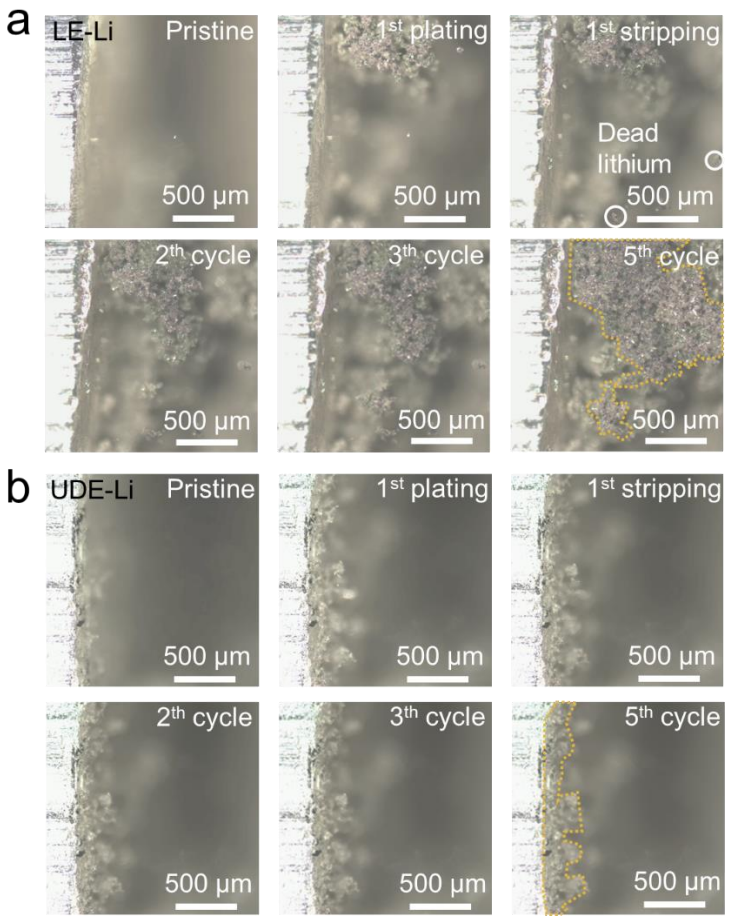

Supplementary Fig. 36|Observation of Li plating and stripping behavior. a,b, In-situ optical microscopy (OM) analysis of Li||Li cells using LE-1 electrolyte (**a**)**,** and UDE-1 electrolyte (**b**) at the 1st, 2th, 3th, and 5th cycles.

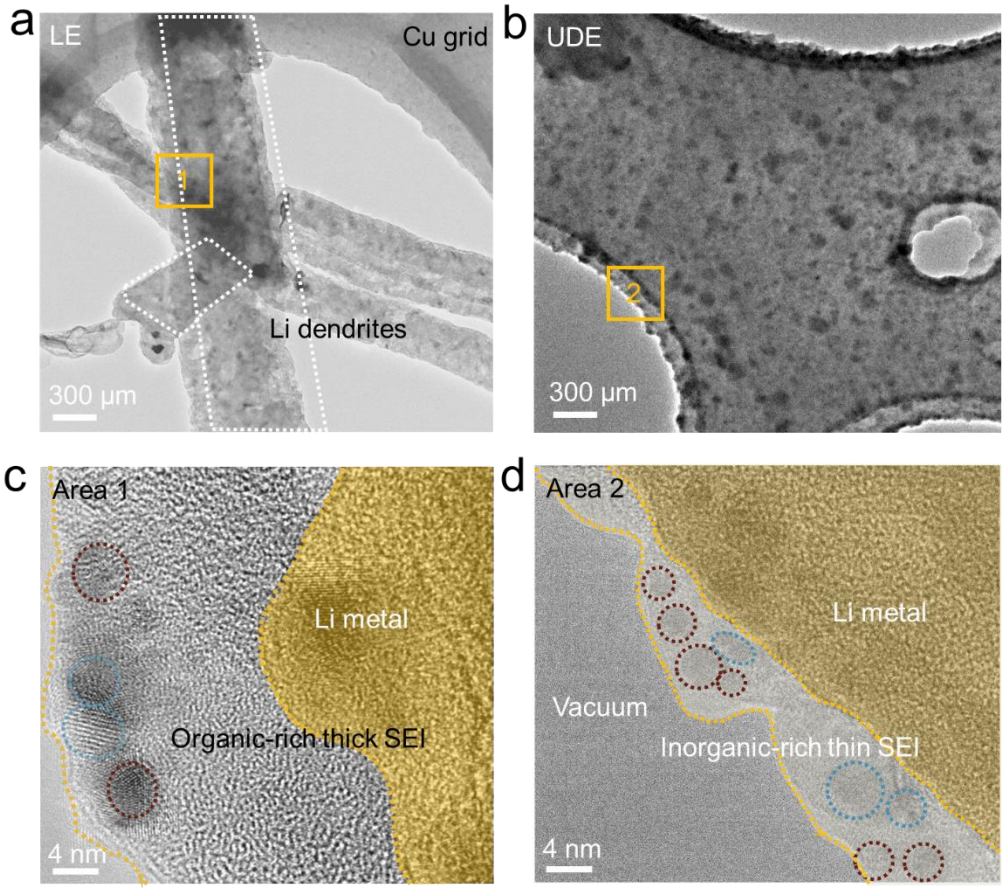

Supplementary Fig. 37|Microstructures observation of Li plating with different electrolytes. Li deposited on the Cu grid at the current density of 0.5 mA cm^{-2} for 15 min using LE1 electrolyte (**A, C**) and UDE1 electrolyte (**B, D**).

Supplementary Note 9

The evolution of the (003) diffraction peak is closely related to changes in the lattice parameter *c* of layered cathodes. At elevated voltages, a more pronounced shift of the (003) diffraction peak is observed in LE-NCM811 compared to UDE-NCM811, suggesting that the UDE electrolyte significantly enhances the reversibility of structural changes during cycling. This improvement in structural stability is likely a consequence of the delocalized UDE electrolyte, which promotes the formation of a stable and robust inorganic cathode-electrolyte interface (CEI). The ability of the UDE electrolyte to maintain structural integrity under high-voltage cycling underscores its potential to mitigate degradation mechanisms, thereby improving the long-term performance and cycle life of cathode.

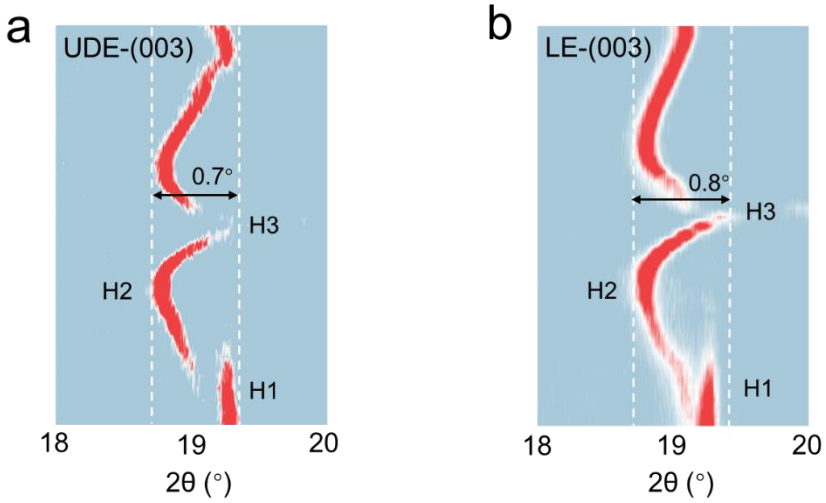

Supplementary Fig. 38|In-situ X-ray diffraction (XRD) evolution of NCM811cathodes with different electrolytes at the (003) diffraction peak during the first cycle at 0.2 C. a, LE1 electrolyte. **b,** UDE1 electrolyte.

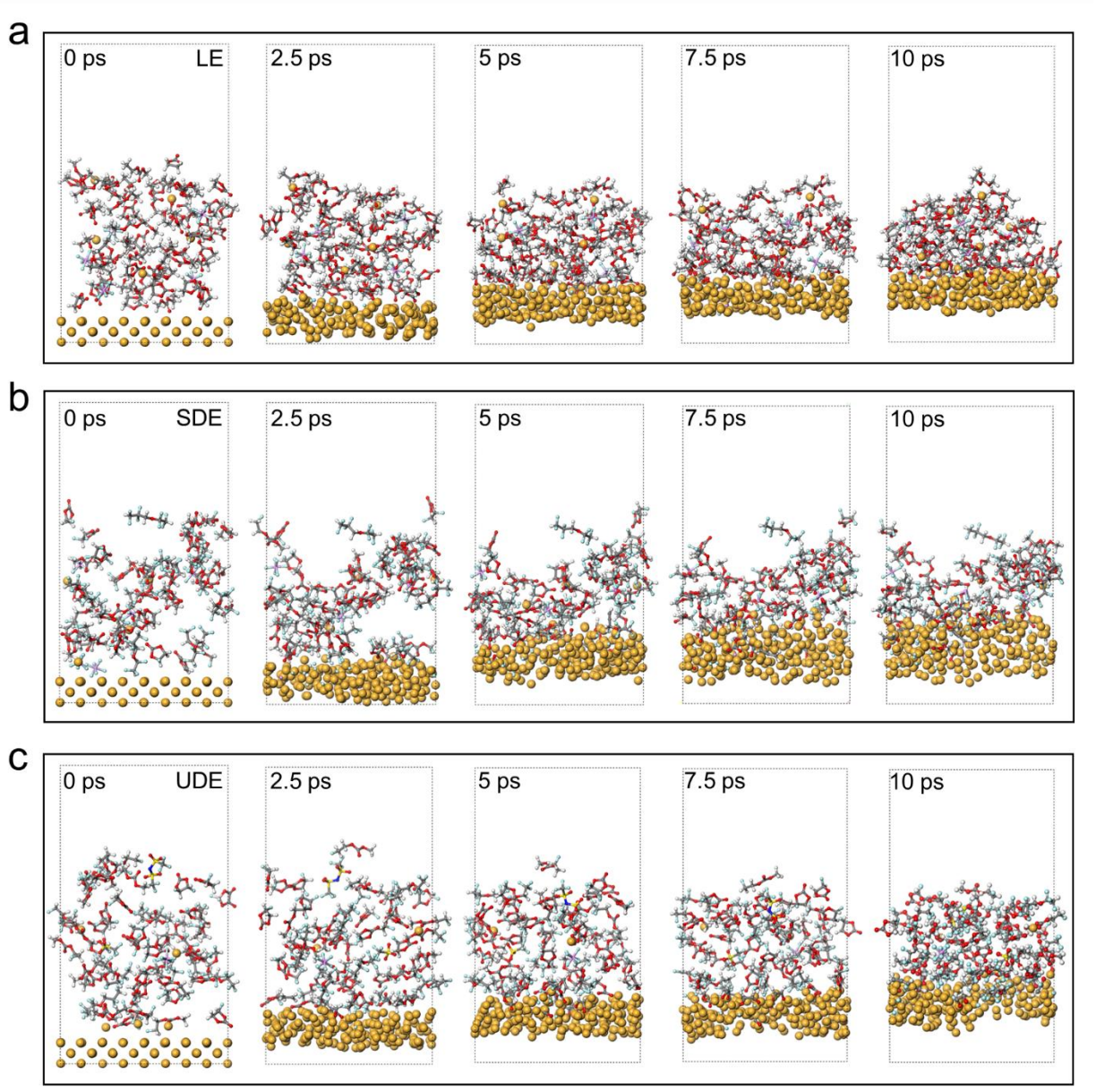

Supplementary Fig. 39|AIMD simulations of interfacial decomposition reaction for different electrolytes on Li anode. a, LE1 electrolyte. **b,** SDE1 electrolyte. **c,** UDE1 electrolyte after 0 ps, 2.5 ps, 5 ps, 7.5 ps, and 10 ps AIMD simulation. Note that all results are presented in the original style to reflect reaction differences.

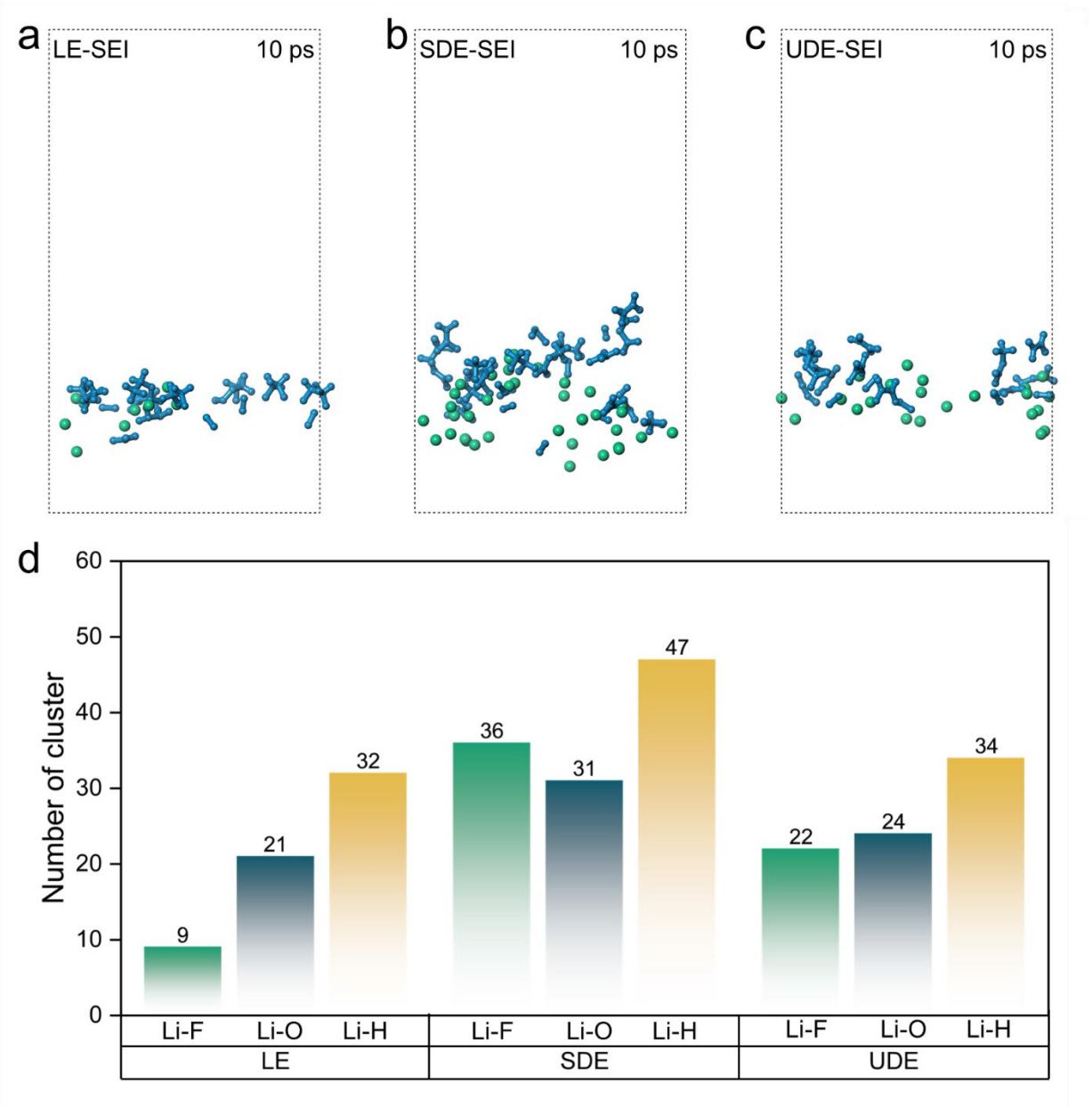

Supplementary Fig. 40|SEI component analysis. a-c, AIMD simulations results of LE-SEI (**a**), SDE-SEI (**b**), and UDE-SEI (**c**) after 10 ps. **d,** Contents of Li-F (LiF), Li-O (organic components), and Li-H (organic components) species formed by different electrolytes on Li anodes.

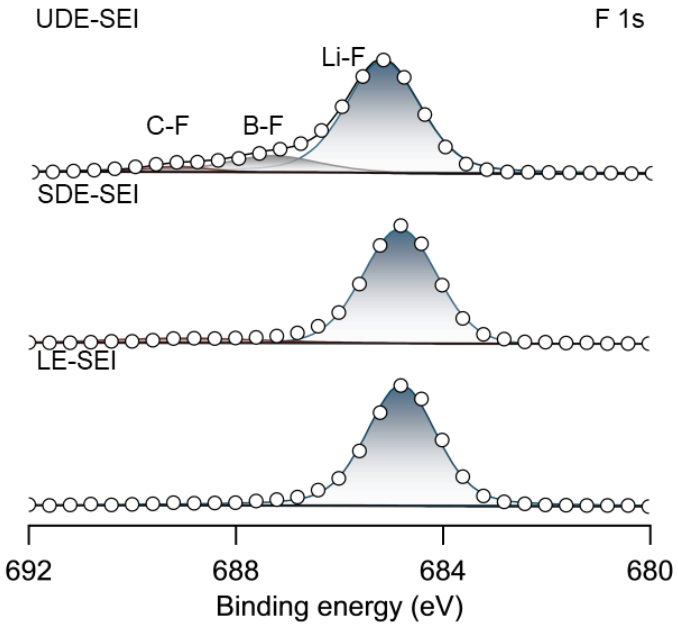

Supplementary Fig. 41|C 1s X-ray photoelectron spectroscopy (XPS) spectra of cycled lithium anodes using UDE, SDE, and LE electrolytes.

Supplementary Note 10

The structure of the solid electrolyte interphase (SEI) was elucidated using time-of-flight secondary ion mass spectrometry (ToF-SIMS). Analysis reveals that the SEI formed in the LE electrolyte is predominantly organic in composition, as evidenced by the high intensity of the $C_2H_3O^-$ fragment signal. In contrast, the SEI generated in the UDE electrolyte displays a markedly inorganic-rich profile, characterized by a strong LiF_2^- signal along with other notable inorganic fragments, such as BO_2^- and SO_2^-(Supplementary Figs. 41 and 42). Furthermore, as sputtering time increases, distinct differences in SEI thickness between the two electrolytes become visually apparent, with UDE-SEI exhibiting a more compact and robust structure (Supplementary Fig. 43). These observations underscore the role of the UDE electrolyte in promoting the formation of a stable, inorganic-dominated SEI, which is critical for enhancing the long-term stability and performance of LMBs.

Similarly, the cathode-electrolyte interphase (CEI) formed in the UDE electrolyte is rich in inorganic components, as evidenced by the strong presence of the LiF_2^- fragment alongside other significant inorganic species, such as BO_2^-. This inorganic-dominated composition indicates a stable CEI layer, which is likely to enhance the electrochemical and structural resilience of the cathode during cycling. The formation of this robust, inorganic-rich CEI highlights the effectiveness of the UDE electrolyte in providing superior interface stability, thereby contributing to improved battery longevity and high-voltage performance.

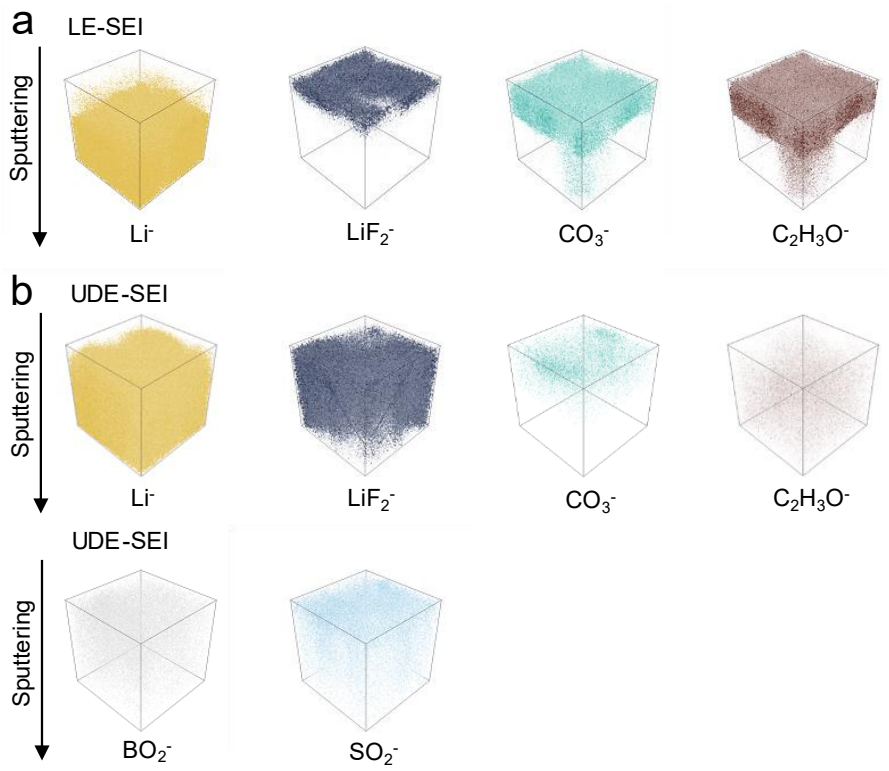

Supplementary Fig. 42|The 3D nanostructure of SEI. a, The Li^-, LiF_2^-, CO_3^-, and $C_2H_3O^-$ fragments in LE-SEI. **b,** The Li^-, LiF_2^-, CO_3^-, $C_2H_3O^-$, BO_2^-, and SO_2^- fragments in LE-SEI.

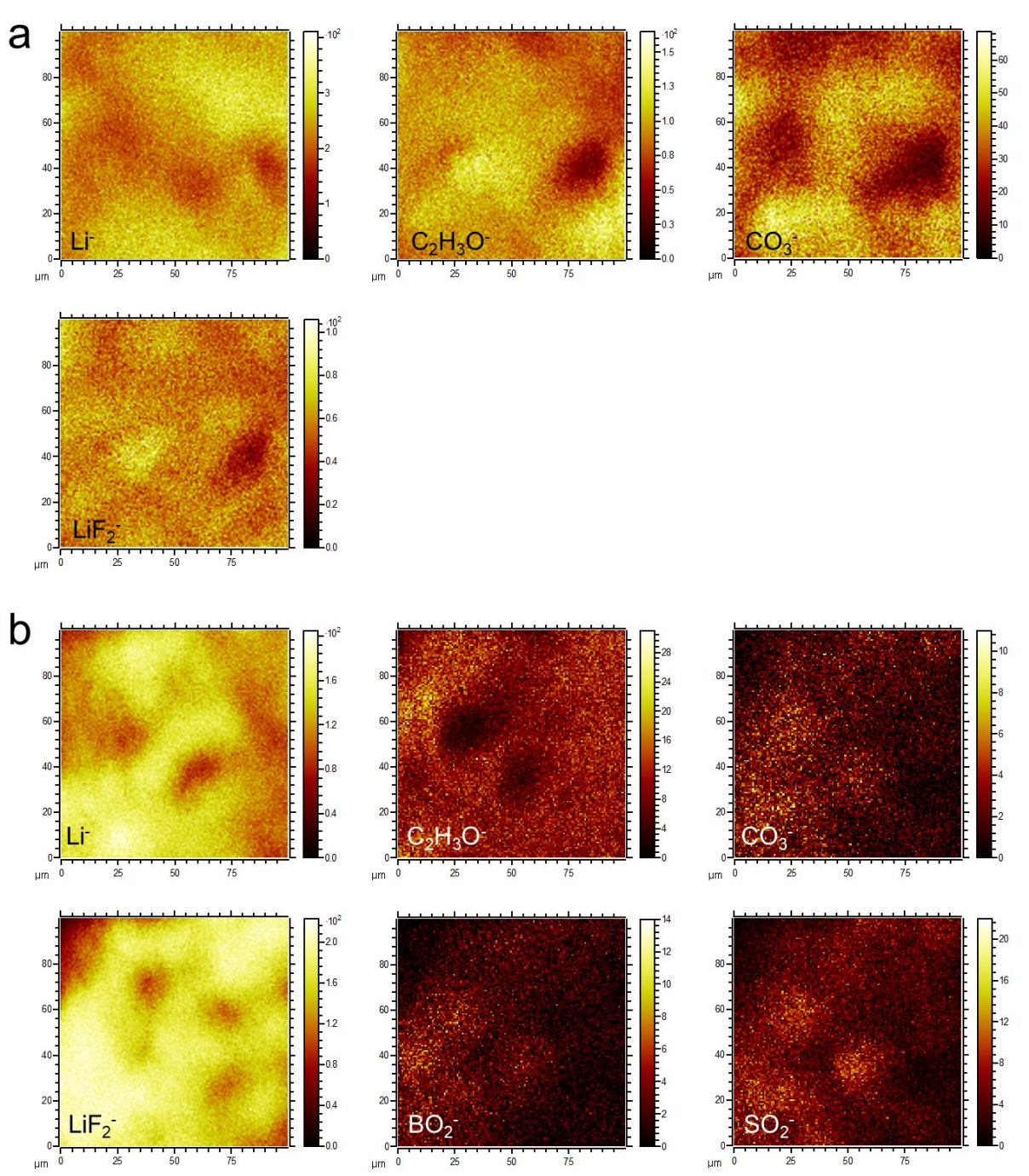

Supplementary Fig. 43|Surface ToF-SIMS component mapping of cycled Li metal anodes for different electrolytes. a, LE electrolyte. **b,** UDE electrolyte.

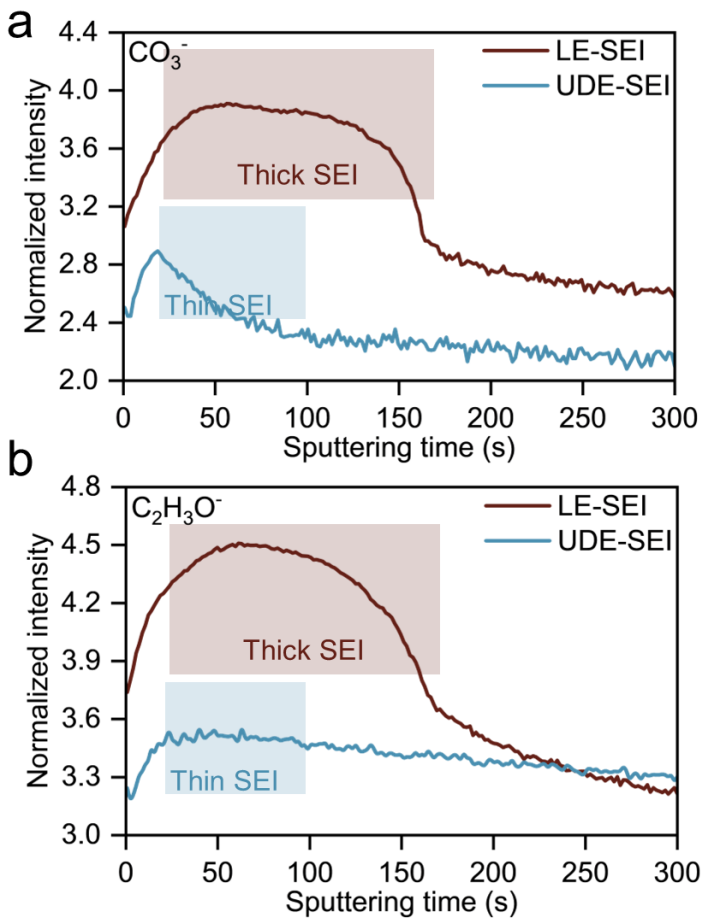

Supplementary Fig. 44|The corresponding ToF-SIMS depth data for LE-SEI and UDE-SEI. **a,** The depth profiles for CO_3^-. **b,** The depth profiles for $C_2H_3O^-$. **c,** The relative composition of Li^-, LiF_2^-, CO_3^-, and $C_2H_3O^-$ species. Normalized intensity is obtained through log (intensity) conversion.

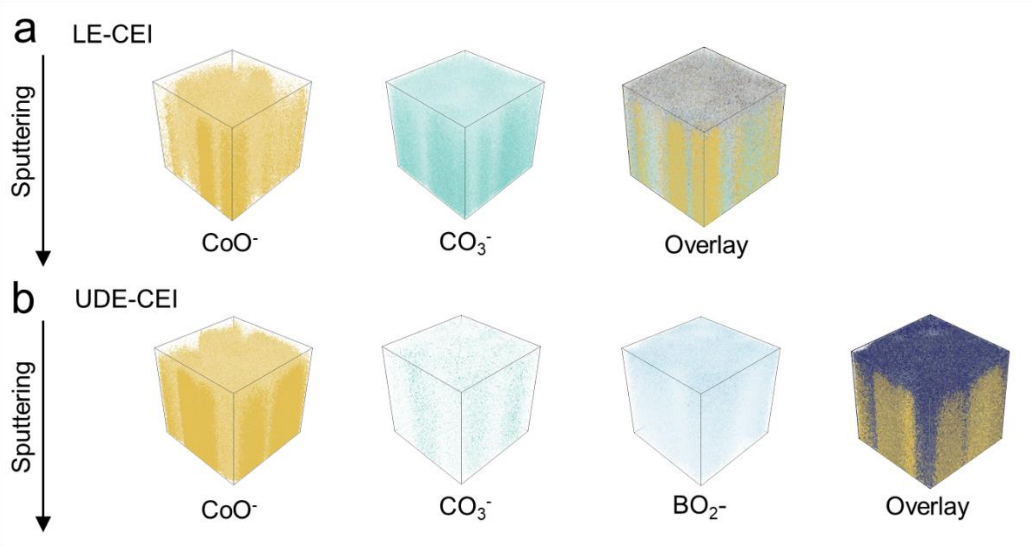

Supplementary Fig. 45|The 3D nanostructure of CEI. a, The CoO^- and CO_3^-fragments with the corresponding overlay for LE-CEI. **b,** The CoO^-, CO_3^-, and BO_2^- fragments with the corresponding overlay for UDE-CEI.

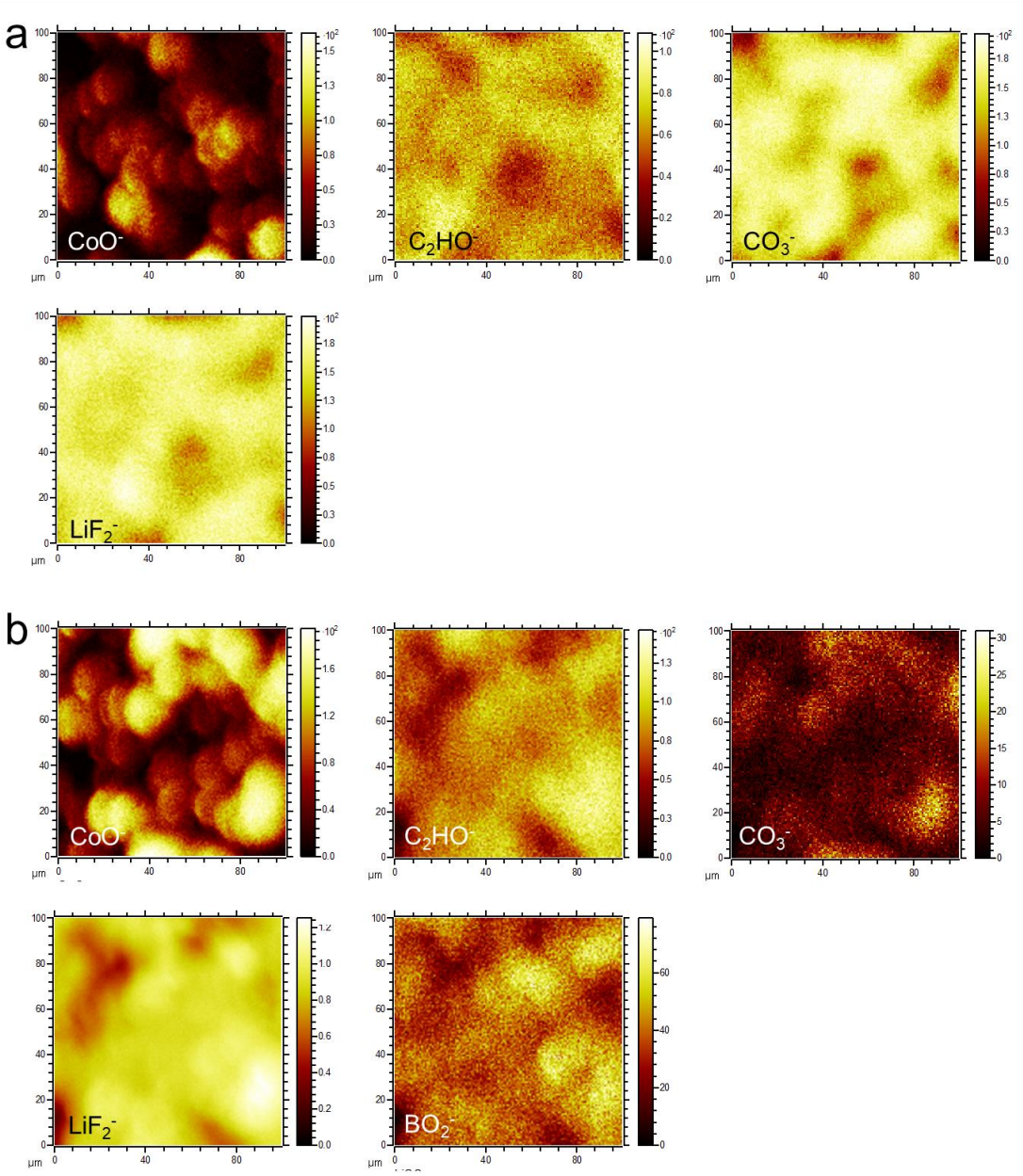

Supplementary Fig. 46|Surface ToF-SIMS component mapping of cycled NCM811 cathodes for different electrolytes. a, LE electrolyte. **b,** UDE electrolyte.

Supplementary Table 1|Summary of all solvent data for screening

Solvent	HOMO (eV)	LUMO (eV)	Solvation energy (eV)	Cluster
Carbonocyanidic amide $C_2H_2N_2O$	-8.65	-2.1	-1.89	1 (Target)
3-Oxopropanenitrile C_3H_3NO	-8.23	-2.08	-1.48	1
1-Fluoro-2-(methylsulfonyl)benzene (FS) $C_7H_7FO_2S$	-7.74	-1.72	-2.42	1
Methyl benzenesulfonate $C_7H_8O_3S$	-7.8	-1.67	-2.35	1
Prop-1-ene-1,3-sultone $C_3H_4O_3S$	-8.21	-1.66	-2.21	1
Ethyl vinyl sulfone (EVS) $C_4H_8O_2S$	-8.08	-1.55	-2.46	1
N-Cyanoformamide $C_2H_2N_2O$	-8.55	-1.54	-1.65	1
3-Oxobutanenitrile C_4H_5NO	-7.86	-1.47	-2.4	1
2-Oxo-1,3-dioxolane-4-carbonitrile $C_4H_3NO_3$	-9.11	-1.3	-1.98	1
Methyl 2,2,2-trifluoroethyl carbonate (TFEMC) $C_4H_5F_3O_3$	-9.11	-1.3	-1.98	1
Ethylene sulfite (ES) $C_2H_4O_3S$	-8.21	-1.24	-2.14	1
Methyl 2,2,2-trifluoroethyl carbonate (FEMC) $C_4H_5F_3O_3$	-8.65	-1.22	-2.27	1
Propylene sulfite (PS) $C_3H_6O_3S$	-8.08	-1.18	-2.21	1
Ethyl difluoroacetate (EDFA) $C_4H_6F_2O_2$	-8.4	-1.14	-2.18	1
Fluoroacetonitrile C_2H_2FN	-9.78	-1.14	-1.73	1
Trifluoroacetamide $C_2H_2F_3NO$	-8.33	-1.08	-2	1

Glycolonitrile C_2H_3NO	-8.71	-1.03	-1.97	1
Cyanoacetic acid C_3H_3NO	-8.8	-1.02	-2.22	1
3-Cyanopropane-1-sulfonyl fluoride (CPSF) $C_4H_6FNO_2S$	-9.61	-0.98	-2.62	1
Malononitrile (MAN) $C_3H_2N_2$	-9.89	-0.95	-1.66	1
Chloromethylsulfonylmethane $C_2H_5ClO_2S$	-8.41	-0.87	-2.25	1
Methanesulfonyl fluoride (FMS) CH_3FO_2S	-9.52	-0.86	-1.57	1
Glutaronitrile (GLN) $C_5H_6N_2$	-9.4	-0.8	-1.9	1
1,1,1-Trifluoro-2-methylsulfony-lethane (FEMS) $C_3H_5F_3O_2S$	-8.74	-0.7	-2.19	1
Difluoroethylene carbonate (DFEC) $C_3H_2F_2O_3$	9.46	-0.66	-1.37	1
Methyl 2-cyano-2-methylpropanoate $C_6H_9NO_2$	-8.22	-0.65	-1.82	1
Methyl 3,3,3-trifluoropropionate (TFPM) $C_4H_5F_3O_2$	-8.41	-0.64	-1.83	1
Methyl(fluoromethyl) sulfone $C_2H_5FO_2S$	-8.48	-0.63	-2.2	1
3,3,3-Trifluoropropanenitrile $C_3H_2F_3N$	-9.95	-0.63	-1.76	1
Fluoroethylene carbonate (FEC) $C_3H_3FO_3$	-9	-0.6	-2.06	1
Adiponitrile (ADN) $C_6H_8N_2$	-9.28	-0.6	-1.95	1
Trifluoromethanesulphonylethane (FMES) $C_3H_5F_3O_2S$	-8.87	-0.6	-1.91	1
Pimelonitrile (PMN) $C_7H_{10}N_2$	-9.15	-0.57	-2.02	1

Ethyl 3,3,3-trifluoropropanoate (TFPE) $C_5H_7F3O_2$	-8.3	-0.57	-1.78	1
1,1,1-Trifluoro-3-(methylsulfonyl) propane (FPMS) $C_4H_7F_3O_2S$	-8.57	-0.54	-2.12	1
Difluoro(methylsulfonyl)methane $C_2H_4F_2O_2S$	-8.68	-0.53	-1.98	1
3-Fluoro-1,3-propane sultone $C_3H_5FO_3S$	-8.88	-0.51	-1.99	1
Methyl (3-(methylsulfonyl)propyl) carbonate (MSPMC) $C_6H_{12}O_5S$	-8.27	-0.49	-1.96	1
Suberonitrile (SUN) $C_8H_{12}N_2$	-9.06	-0.48	-2.04	1
2-(Trifluoromethanesulfonyl)propane (FMIS) $C_4H_7F_3O_2S$	-8.67	-0.47	-2.01	1
Carbamic fluoride CH_2FNO	-8.66	-0.47	-1.98	1
Azelanitrile (AZN) $C_9H_{14}N$	-8.97	-0.45	-2.08	1
Methyltrifluoromethyl sulfone $C_2H_3F_3O_2S$	-9.07	-0.45	-1.8	1
4-(Fluoromethyl)-1,3-dioxolan-2-one (FPC) $C_4H_5FO_3$	-8.65	-0.44	-2.22	1
Bis(2,2,2-trifluoroethyl)carbonate (HFDEC) $C_5H_4F_6O_3$	-9.29	-0.43	-1.46	1
Bis(2,2,2-trifluoroethyl) ether (BTFE) $C_4H_4F_6O$	-8.77	-0.42	-1.75	1
Sebaconitrile (SEN) $C_{10}H_{16}N_2$	-8.89	-0.39	-2.09	1
Propanenitrile C_3H_5N	-9.12	-0.36	-2.1	1
Acetonitrile (ACN) C_2H_3N	-9.27	-0.31	-2.03	1

Butanenitrile C_4H_7N	-9.05	-0.25	-2.13	1
Methyl 2,2,3,3,3-pentafluoropropyl carbonate (PFPMC) $C_5H_5F_5O_3$	-8.78	-0.24	-1.74	1
Trimethylacetonitrile C_5H_9N	-8.96	-0.22	-2.19	1
Pentanenitrile C_5H_9N	-8.98	-0.21	-2.15	1
2,2-Dimethylbutanenitrile $C_6H_{11}N$	-8.86	-0.17	-2.21	1
1,1,2,2-Tetrafluoroethyl 2,2,2-trifluoroethyl ether (HFE) $C_4H_2F_8O$	-10.01	-0.17	-1.74	1
Ethyl 1,1,2,2-tetrafluoroethyl ether (ETFE) $C_4H_6F_4O$	-10.04	-0.16	-1.74	1
2,2-Difluoroethyl ethyl carbonate (EDFEC) $C_5H_8F_2O_3$	-8.54	-0.14	-1.85	1
Carbonic acid methyl 3,3,3-trifluoropropyl ester (TrFPMC) $C_5H_7F_3O_3$	-8.51	-0.1	-1.92	1
1,1,2,2-Tetrafluoro-3-(1,1,2,2tetrafluoroethoxy) propane (FEPE/TTE) $C_5H_4F_8O$	-9.14	-0.05	-1.73	1
4,4-Difluoro-1,3-Dioxane $C_4H_6F_2O_2$	-8.36	-0.04	-1.48	1
Difluoro(dimethoxy)methane $C_3H_6F_2O_2$	-8.64	-0.03	-1.81	1
2-Oxo-1,3-dioxolane-4-carboxylic acid $C_4H_4O_5$	-8.27	-0.02	-2.72	1
Trifluoro(methoxymethoxy)methane $C_3H_5F_3O_2$	-8.49	-0.01	-1.9	1

4-Trifluoromethyl-1,3-dioxolan-2-one (TFPC) $C_4H_3F_3O_3$	-8.68	0.01	-2.24	1
1-Fluoroethyl Methyl Carbonate (1FEMC) $C_4H_7FO_3$	-8.54	0.02	-2.86	1
2,2-Difluoroethyl methyl carbonate (DFEMC) $C_4H_6F_2O_3$	-8.12	0.07	-2.12	1
1,1,2,2-Tetrafluoroethyl-2,2,2-trifluoroethyl ether (TFTFE) $C_4H_3F_7O$	-7.14	0.21	-2	1
2-(Methylsulfonyl)ethyl 2,2,2-trifluo-roacetate (MSTFA) $C_5H_7F_3O_4S$	-8.65	-1.64	-2.8	2
2-Methanesulfonylethyl 2,2-difluoroacetate (MSPTFA) $C_5H_8F_2O_2S$	-8.53	-1.42	-3.11	2
Methyl (methylsulfonyl)acetate (MMSA) $C_4H_8O_4S$	-8.21	-1.15	-3.13	2
N,N-Dimethylbenzamide $C_9H_{11}NO$	-6.72	-1.1	-2.75	2
Ethyl methanesulfonylacetate (EMSA) $C_5H_{10}O_4S$	-8.12	-1.09	-3.19	2
Chloroacetone C_3H_5ClO	-6.74	-0.86	-2.36	2
Methoxyacetone $C_4H_8O_2$	-7.08	-0.78	-3	2
Ethyl 2-cyano-2-methylpropanoate $C_7H_{11}NO_2$	-8.15	-0.74	-2.63	2

Ethyl 2-fluorosulfonylethyl carbonate (EFSEC) $C_5H_9FO_5S$	-8.61	-0.73	-2.86	2
Butyl ethyl ketone $C_7H_{14}O$	-6.92	-0.63	-2.28	2
2-Fluoroacetamide C_2H4FNO	-7.6	-0.53	-2.65	2
N-Fluoromethyl-N-methylformamide C_3H_6FNO	-7.66	-0.52	-2.48	2
Methanesulfonyl(methoxy)methane (MMMS) $C_3H_8O_3S$	-8.08	-0.5	-2.62	2
2-Fluoro-N-methylacetamide C_3H_6FNO	-7.47	-0.49	-2.79	2
2-(Methylsulfonyl)ethyl acetate (MSEA) $C_5H_{10}O_4S$	-8.01	-0.48	-3.24	2
Delta-Valerolactone (DVL) $C_5H_8O_2$	-7.47	-0.46	-2.49	2
Diethyl sulfone (DES) $C_4H_{10}O_2S$	-7.94	-0.42	-2.52	2
Ethyl isobutyl sulfone (EiBS) $C_6H_{14}O_2S$	-7.68	-0.41	-2.57	2
Dipropyl sulfone (DPS) $C_6H_{14}O_2S$	-7.75	-0.41	-2.56	2
3-Methoxysulfolane (MESL) $C_5H_{10}O_3S$	-7.83	-0.41	-2.45	2
4,5-Dimethyl-1,3-dioxol-2-one $C_5H_6O_3$	-6.73	-0.41	-2.33	2
1-(Ethanesulfonyl)-2-methoxyethane (EMES) $C_5H_{12}O_3S$	-7.39	-0.4	-3.25	2
Urea CH_4N_2O	-7.38	-0.4	-2.59	2
Methyl 3,3-difluoropropanoate $C_4H_6F_2O_2$	-8.06	-0.39	-2.61	2
3-Methylsulfolane (3MESL) $C_5H_{10}O_2S$	-7.85	-0.39	-2.51	2

1-Methoxy-2(2methoxyethanesulfon-yl) ethane (DMES) $C_6H_{14}O_4S$	-7.33	-0.38	-3.24	2
Formylhydrazine CH_4N_2O	-7.27	-0.38	-2.82	2
Methyl 3-fluoropropanoate $C_4H_7FO_2$	-8.01	-0.38	-2.66	2
Ethyl isopropyl sulfone (EiPS) $C_5H_{12}O_2S$	-7.79	-0.38	-2.59	2
2-Methoxyacetamide $C_3H_7NO_2$	-7.24	-0.37	-3.24	2
2-(Ethylsulfonyl)butane (EsBS) $C_6H_{14}O_2S$	-7.75	-0.37	-2.63	2
2-Fluoro-N, N-dimethylacetamide C_4H_8FNO	-7.08	-0.36	-2.93	2
2-Methyl-1-(propane-2-sulfonyl) propane (IPiBS) $C_7H_{16}O_2S$	-7.69	-0.36	-2.63	2
2-(Propane-2-sulfonyl)butane (IPSBS) $C_7H_{16}O_2S$	-7.68	-0.36	-2.63	2
Isopropyl Methyl Sulfone (MiPS) $C_4H_{10}O_2S$	-7.91	-0.36	-2.5	2
Methyl propyl sulfone (MPS) $C_4H_{10}O_2S$	-8.05	-0.36	-2.47	2
Tetramethylene sulfone (TMS/Sulfolane) $C_4H_8O_2S$	-7.89	-0.36	-2.47	2
3-Isopropoxytetrahydrothiophene 1,1-dioxide (ISEL) $C_7H_{14}O_3S$	-7.64	-0.35	-2.49	2
3-Ethoxysulfolane (EESL) $C_6H_{12}O_3S$	-7.71	-0.34	-2.47	2
3-(2-Methoxyethoxy)thiolane 1,1-dioxide (GLSL) $C_7H_{14}O_4S$	-7.58	-0.31	-2.45	2
Methyl glycinate $C_3H_7NO_2$	-6.82	-0.3	-2.93	2
3-Fluoropropanamide C_3H_6FNO	-7.39	-0.27	-2.87	2

Isobutyramide C_4H_9NO	-7.07	-0.27	-2.53	2
Propylamide (Propanamide) C_3H_7NO	-7.14	-0.27	-2.49	2
Acetamide C_2H_5NO	-7.17	-0.27	-2.48	2
Dimethyl methylphosphonate (DMMP) $C_3H_9PO_3$	-8.01	-0.26	-2.78	2
Butanamide C_4H_9NO	-7.14	-0.26	-2.5	2
N-methylacetamide (NMA) C_3H_7NO	-7.04	-0.24	-2.58	2
2-Fluoroethyl acetate (2FEA) $C_4H_7FO_2$	-7.94	-0.22	-2.66	2
N-Ethylformamide C_3H_7NO	-7.1	-0.22	-2.57	2
N-methyl-2-oxazolidinone $C_4H_7NO_2$	-7.14	-0.21	-2.59	2
N,N-diethylacetamide $C_6H_{13}NO$	-6.67	-0.2	-2.72	2
N,N-dimethylpropionamide $C_5H_{11}NO$	-6.69	-0.18	-2.68	2
Dimethyl acetamide (DMA) C_4H_9NO	-6.74	-0.17	-2.65	2
2-Pyrrolidinone C_4H_7NO	-6.92	-0.17	-2.6	2
Methoxymethyl acetate $C_4H_8O_3$	-7.7	-0.16	-2.77	2
Dimethyl sulfoxide (DMSO) C_2H_6OS	-6.5	-0.16	-2.72	2
Dimethyl formamide (DMF) C_3H_7NO	-6.96	-0.16	-2.52	2
1-Methylimidazole $C_4H_6N_2$	-6.42	-0.16	-2.49	2
N,N-Dimethylbutyramide $C_9H_{11}NO$	-6.69	-0.15	-2.72	2
Diethyl sulfoxide (DESO) $C_4H_{10}SO$	-6.32	-0.14	-2.79	2
N-Methylformamid C_2H_5NO	-7.29	-0.13	-2.47	2
Trimethyl phosphate (TMP) $C_3H_9PO_4$	-7.97	-0.11	-2.84	2
Triethyl phosphate (TEP) $C_6H_{15}PO_4$	-7.97	-0.11	-2.76	2

Methyl methoxyacetate (MMOA) $C_4H_8O_3$	-7.52	-0.09	-2.98	2
Dipropyl sulfoxide (DPSO) $C_6H_{14}SO$	-6.29	-0.09	-2.87	2
1-Methyl-2-pyrrolidinone (NMP) C_5H_9NO	-6.73	-0.08	-2.67	2
N-methylpyrrolidinone C_5H_9NO	-6.73	-0.08	-2.67	2
Dibutyl sulfoxide (DBSO) $C_8H_{18}OS$	-6.26	-0.07	-2.9	2
Methoxy(methoxymethoxy)methane $C_4H_{10}O_3$	-6.95	-0.07	-2.01	2
1-Ethoxy-2-(2,2,2-trifluoroethoxy) ethane (ETFEE) $C_6H_{11}F_3O_2$	-7.33	-0.04	-3.08	2
N,N'- dimethylimidazolidinone $C_5H_{10}N_2O$	-6.48	-0.04	-2.72	2
Ethyl fluoroethyl carbonate (EFEC) $C_5H_9FO_3$	-8.35	-0.03	-2.03	2
2-Fluoropropyl methyl carbonate (2FPMC) $C_5H_9FO_3$	-8.29	-0.02	-2.77	2
1,3-Dioxan-2-Amine $C_4H_9NO_2$	-7.05	0.03	-2.81	2
Dimethoxymethane (DMM) $C_3H_8O_2$	-7.17	0.05	-2.69	2
Diisopropyl ether $C_6H_{14}O$	-6.93	0.08	-2.26	2
Fluoromethoxy(methoxy)methane $C_3H_7FO_2$	-8.08	0.09	-2.44	2
Ethanethioamide C_2H_5NS	-5.89	-1.18	-1.97	3
2-Pyrrolidinethione C_4H_7NS	-5.72	-0.96	-2	3
Dimethylketone C_3H_6O	-7.05	-0.76	-2.15	3
3,4-Difluorofuran $C_4H_2F_2O$	-7.05	-0.7	-1.03	3
2-Butanone (methyl ethyl ketone) C_4H_8O	-7	-0.69	-2.2	3
2,3-Difluorofuran $C_4H_2F_2O$	-6.78	-0.52	-1.13	3
Methoxybenzene C_7H_8O	-6.23	-0.46	-1.73	3

3-Fluorofuran C_4H_3FO	-6.76	-0.46	-1.12	3
Phenetole $C_8H_{10}O$	-6.19	-0.42	-1.95	3
Butyl phenyl ether $C_{10}H_{14}O$	-6.17	-0.41	-2.02	3
Propoxybenzene $C_9H_{12}O$	-6.17	-0.41	-1.99	3
2,4-Difluorofuran $C_4H_2F_2O$	-6.84	-0.39	-1.13	3
Aminomethylal $C_3H_9NO_2$	-8.01	-0.38	-2.66	3
2-Fluorofuran C_4H_3FO	-6.59	-0.2	-1.32	3
2,5-Difluorofuran $C_4H_2F_2O$	-6.65	-0.18	-1.18	3
Furan C_4H_4O	-6.53	-0.17	-1.38	3
3-Methoxyfuran $C_5H_6O_2$	-5.95	-0.13	-1.5	3
2-Ethylfuran C_6H_8O	-6.16	-0.1	-1.62	3
1-(2,2,2-Trifluoroethoxy)-2-methoxyethane (TFEME) $C_5H_9F_3O_3$	-7.68	-0.01	-1.24	3
2-Methoxyfuran $C_5H_6O_2$	-5.82	0.01	-2.01	3
Methyl tert-butyl ether $C_5H_{12}O$	-7.02	0.04	-2.19	3
3-Methyltetrahydrofuran $C_5H_{10}O$	-6.81	0.05	-2.12	3
5-Methoxy-1,3-Dioxane $C_5H_{10}O_3$	-7.12	0.06	-1.73	3
Cyclopentyl methyl ether $C_6H_{12}O$	-6.98	0.09	-2.13	3
1-(2,2-Difluoroethoxy)-2-ethoxyethane (EDFEE) $C_6H_{12}F_2O_2$	-7.41	0.09	-1.85	3
2,3-Dimethylfuran C_6H_8O	-5.99	0.09	-1.61	3
2-Methyl tetrahydrofurane (2-Me-THF) $C_5H_{10}O$	-6.81	0.1	-2.18	3

2-Methyltetrahydrofuran $C_5H_{10}O$	-6.81	0.1	-2.18	3
4-Methyl-1,3-dioxolane (4ME13DOL) $C_4H_8O_2$	-7.14	0.1	-1.79	3
Tetrahydrofuran (THF) C_4H_8O	-6.82	0.11	-2.09	3
Tetrahydropyran $C_5H_{10}O$	-6.95	0.12	-2.05	3
Tetrahydropyran $C_5H_{10}O$	-6.95	0.12	-2.05	3
1-(2-Fluoroethoxy)-2-ethoxyethane (EFEE) $C_6H_{13}FO_2$	-7.33	0.12	-1.67	3
1-(2-Fluoroethoxy)-2-methoxyethan (FEME) $C_5H_{11}FO_2$	-7.4	0.12	-1.64	3
2,5-Dimethylfuran C_6H_8O	-5.84	0.12	-1.62	3
Dioxolane (1,3-dioxolane) $C_3H_6O_2$	-7.22	0.13	-1.68	3
2-Methyl-1,3-dioxolane (2ME13DOL) $C_4H_8O_2$	-7.31	0.15	-1.84	3
1-Ethoxy-2-methoxyethane $C_5H_{12}O_2$	-7.64	0.16	-2.56	3
Ethoxymethoxymethane $C_4H_{10}O_2$	-7.58	0.16	-1.85	3
Triglyme $C_8H_{18}O_4$	-7.19	0.19	-1.92	3
Diglyme $C_6H_{14}O_3$	-7.18	0.19	-1.9	3
Diethyl ether $C_4H_{10}O$	-7.1	0.21	-2.1	3
1,2-Diethoxyethane (DEE) $C_6H_{14}O_2$	-7.1	0.21	-2.03	3
1-Ethoxy-2-methoxyethane (EME) $C_5H_{12}O_2$	-7.14	0.21	-2	3
2-Methyl-1,4-dioxane $C_5H_{10}O_2$	-6.75	0.22	-1.96	3
1,2-Dimethoxy ethane (DME) $C_4H_{10}O_2$	-7.19	0.22	-1.88	3

Dioxane $C_4H_8O_2$	-6.81	0.22	-1.83	3
Aminoacetone C_3H_7NO	-8.35	1.18	-2.07	3
1,3-Benzodioxol-2-one $C_7H_4O_3$	-7.17	-1.27	-2.13	4
Fluoroacetone C_3H_5FO	-7.45	-1.14	-1.99	4
Pyridine C_5H_5N	-7.22	-1.13	-2.13	4
Methyl fluorosulfonyl acetate $C_3H_5FO_4S$	-8.93	-1.1	-2.5	4
Methyl fluorosulfonylacetate (MFSA) $C_3H_5FO_4S$	-8.93	-1.1	-2.5	4
Succinimide $C_4H_5NO_2$	-7.59	-1.08	-2.08	4
Benzyl nitrile (Benzyl cyanide) C_8H_7N	-7.3	-0.98	-2.16	4
2-Fluorobutyrolactone (FGBL) $C_4H_5FO_2$	-8	-0.84	-2.2	4
N,N-dimethyltrifluoroacetamide $C_4H_6F_3NO$	-7.55	-0.82	-2.39	4
Vinyl acetate $C_4H_6O_2$	-7.2	-0.82	-2.04	4
Methyl cyanoacetate (MCA) $C_4H_5NO_2$	-8.55	-0.77	-2.4	4
(Methylsulfonyl)propylacetate (MSPA) $C_6H_{12}O4S$	-7.81	-0.73	-2.38	4
Aminoacetonitrile $C_2H_4N_2$	-7.61	-0.71	-2.08	4
1,1-Dioxothiolan-3-yl acetate (ACSL) $C_6H_{10}O_4S$	-8.07	-0.7	-2.46	4
Ethyl cyanoacetate (ECA) $C_5H_7NO_2$	-8.44	-0.69	-2.48	4
1,1,1-Trifluoro-2-methylsulfonyl-propane (FIMS) $C_4H_7F_3O_2S$	-8.52	-0.65	-2.31	4

1,1-Dioxo-thiolan-3-yl ethyl carbonate (ECSL) $C_7H_{12}O_5S$	-8.07	-0.63	-2.2	4
4-(Methylsulfonyl)butanenitrile (MCPS) $C_5H_9NO_2S$	-8.38	-0.61	-2.25	4
Vinylene Carbonate (VC) $C_3H_2O_3$	-7.39	-0.61	-2.1	4
2-Methylglutaronitrile $C_6H_8N_2$	-9.28	-0.58	-2.77	4
Fluoromethyl propanoate $C_4H_7FO_2$	-8.24	-0.58	-2.26	4
Isobutylene carbonate $C_5H_8O_3$	-7.73	-0.54	-2.08	4
4-Hydroxy-1,3-dioxolan-2-one $C_3H_4O_4$	-8.55	-0.53	-2.27	4
Methyl propyl carbonate (MPC) $C_5H_{10}O_3$	-8.55	-0.53	-2.27	4
Methoxyacetonitrile C_3H_5NO	-8.14	-0.53	-2.01	4
2-Fluoroethyl methyl carbonate (MFEMC) $C_4H_7FO_3$	-8.27	-0.53	-1.8	4
N-Methoxyformamide $C_2H_5NO_2$	-7.6	-0.48	-2.3	4
Methyl formate $C_2H_4O_2$	-8.18	-0.46	-1.95	4
Ethyl 2-fluoropropanoate (E2FP) C_5H_9FO	-7.95	-0.44	-2	4
Dimethyl sulfone (DMS) $C_2H_6O_2S$	-8.25	-0.43	-2.32	4
{[(2-methanesulfonylethoxy)carbonyl] oxy}methane (MSEMC) $C_5H_{10}SO_5$	-8.33	-0.43	-2.09	4
Ethyl (3-(methylsulfonyl)propyl) carbonate (MSPEC) $C_6H_{14}SO_5$	-8.21	-0.43	-2	4
Thiophene, 3-fluorotetrahydro-, 1,1-dioxide (3-FTMS) $C_4H_7FO_2S$	-8.16	-0.42	-2.31	4

Thiophene,2-fluorotetrahydro-,1,1-dioxide (2-FTMS) $C_4H_7FO_2S$	-8.08	-0.42	-2.25	4
Carbonic acid ethyl[2-(methylsulfonyl)ethyl]ester(ethyl 2-methylsulfonyleth-yl carbonate) (MSDEC) $C_6H_{12}O_5S$	-8.28	-0.42	-2.14	4
2-{[(3-methanesulfonylpropoxy) carbonyl]oxy} propane (MSPiPC) $C_7H_{16}SO_5$	-8.2	-0.42	-2.03	4
Ethyl methyl sulfone (EMS) $C_3H_8O_2S$	-8.09	-0.41	-2.42	4
2-{[(2-methanesulfonylethoxy) carbonyl]oxy}propane (MSEiPC) $C_7H_{14}O_5S$	-8.24	-0.41	-2.19	4
1,4-Butane sultone $C_4H_8O_3S$	-8.62	-0.4	-2.28	4
1,3-Propanesultone $C_3H_6O_3S$	-8.37	-0.4	-2.23	4
Ethyl formate $C_3H_6O_2$	-8.06	-0.38	-2.03	4
i-Butyl formate $C_5H_{10}O_2$	-8.04	-0.37	-2.07	4
Ethyl fluoroacetate (EFA) $C_4H_7FO_2$	-8.11	-0.36	-2.09	4
n-Propyl formate $C_4H_8O_2$	-8.04	-0.36	-2.05	4
Thietane 1,1-dioxide (TriPS) $C_3H_6O_2S$	-8.16	-0.35	-2.31	4
n-Butyl formate $C_5H_{10}O_2$	-8.02	-0.35	-2.07	4
2-Methylthietane 1,1-dioxide (MTS) $C_4H_8O_2S$	-7.95	-0.34	-2.4	4
Gamma-Valerolactone $C_5H_8O_2$	-7.59	-0.33	-2.41	4
i-Propyl formate $C_4H_8O_2$	-7.99	-0.33	-2.08	4

Methyl(2-methoxyethyl) sulfone (MEMS) $C_4H_{10}O_3S$	-7.63	-0.31	-2.37	4
Propylene carbonate (PC) $C_4H_6O_3$	-8.36	-0.31	-2.35	4
Methoxypropionitrile C_4H_7NO	-8.05	-0.3	-2	4
2,3-Butylene carbonate $C_5H_8O_3$	-8.26	-0.28	-2.42	4
Ethylene carbonate (EC) $C_3H_4O_3$	-8.46	-0.28	-2.28	4
1,2-Butylene carbonate (BC) $C_5H_8O_3$	-8.34	-0.27	-2.37	4
Carbamic acid CH_3NO_2	-8.03	-0.27	-2.18	4
2-Fluoroethyl propionate (2FEP) $C_5H_9FO_2$	-8.02	-0.27	-2.07	4
Fluoromethyl methyl carbonate (MFDMC) $C_3H_5FO_3$	-8.05	-0.24	-2.11	4
Butyrolactone (GBL) $C_4H_6O_2$	-7.66	-0.23	-2.34	4
Dimethylcarbamylfluoride(Dimethylcarbamic fluoride) C_3H_6FNO	-7.47	-0.23	-2.25	4
Formamide CH_3NO	-7.47	-0.19	-2.31	4
Methyl 2,2,3,3-tetrafluoropropyl carbonate (TeFPMC) $C_5H_6F_4O_3$	-8.73	-0.18	-2.3	4
3-Methoxypropionitrile C_4H_7NO	-7.84	-0.18	-2.06	4
5-Fluoro-1,3-Dioxane $C_4H_7FO_2$	-7.71	-0.17	-2.43	4
Methoxyformamide (Methyl carbamate) $C_2H_5NO_2$	-7.82	-0.13	-2.31	4
Methyl isobutyrate $C_5H_{10}O_2$	-7.66	-0.13	-2.22	4
2-Hydroxyethyl methyl carbonate $C_4H_8O_4$	-8.45	-0.12	-1.92	4

Butyl sultone $C_8H_{18}O_3S$	-8.06	-0.09	-2.44	4
2-Methoxyethyl acetate $C_5H_{10}O_3$	-7.49	-0.09	-2.2	4
5,5-Difluoro-1,3-Dioxane $C_4H_6F_2O_2$	-8	-0.08	-2.07	4
Isoamyl acetate $C_7H_{14}O_2$	-7.65	-0.07	-2.24	4
Methyl acetate (MA) $C_3H_6O_2$	-7.79	-0.07	-2.11	4
i-Propyl acetate $C_5H_{10}O_2$	-7.65	-0.04	-2.24	4
i-Butyl acetate $C_6H_{12}O_2$	-7.68	-0.03	-2.24	4
1-Methoxy-2-propyl acetate (MPA) $C_6H_{12}O_3$	-7.4	-0.02	-2.26	4
Methyl propionate $C_4H_8O_2$	-7.76	-0.02	-2.18	4
Ethyl acetate (EA) $C_4H_8O_2$	-7.7	-0.01	-2.18	4
Methyl butyrate (MB) $C_5H_{10}O_2$	-7.74	0	-2.22	4
3-Fluoropropyl methyl carbonate (FPMC) $C_5H_9FO_3$	-8.24	0	-2.1	4
1-(2,2,2-Trifluoroethoxy)-2-methoxyethane $C_5H_9F_3O_2$	-7.53	0	-1.98	4
n-Butyl acetate $C_6H_{12}O_2$	-7.67	0.01	-2.23	4
n-Propyl acetate $C_5H_{10}O_2$	-7.68	0.01	-2.22	4
Difluoro(methoxymethoxy)methane $C_3H_6F_2O_2$	-8.42	0.01	-2.19	4
Ethyl propionate $C_5H_{10}O_2$	-7.67	0.02	-2.24	4
Ethyl butyrate (EB) $C_6H_{12}O_2$	-7.65	0.03	-2.29	4
Fluoro(dimethoxy)methane $C_3H_7FO_2$	-8.15	0.04	-2.09	4
Ethyl propan-2-yl carbonate (EiPC) $C_6H_{12}O_3$	-8	0.07	-2.2	4

Diethyl carbonate (DEC) $C_5H_{10}O_3$	-8.06	0.07	-2.17	4
Methyl isopropyl carbonate (MiPC) $C_5H_{10}O_3$	-8.08	0.07	-2.13	4
Ethyl methyl carbonate (EMC) C_4H_8O3	-8.14	0.07	-2.1	4
Dimethyl carbonate (DMC) $C_3H_6O_3$	-8.22	0.07	-2.03	4
2-Methoxy-1,3-Dioxane $C_5H_{10}O_3$	-7.42	0.08	-2.37	4
Ethyl propyl carbonate (EPC) $C_6H_{12}O_3$	-8.04	0.08	-2.19	4
1,1-Difluoro-2-(2-methoxyethoxy) ethane (DFEME) $C_5H_{10}F_2O_2$	-7.47	0.09	-2.15	4
Carbonic acid bis(fluoromethyl) ester (DFDMC) $C_3H_4F_2O_3$	-10.9	1.93	-2.04	4

Supplementary Table 2. Summary of all lithium salt data for screening.

Structure	HOMO (eV)	LUMO (eV)	Binding energy(eV)	Cluster
Lithium hexafluoroantimonate $LiSbF_6$	-13.44	-1.3	-5.68	1 (Target)
Lithium hexafluorostannate(IV) Li_2SnF_6	-12.01	-0.53	-6.38	1
Lithium Hexafluorophosphate $LiPF_6$	-10.99	-1.69	-5.98	1
Lithium tetrafluoroborate $LiBF_4L$	-10.57	-1.5	-6.2	1
Lithium hexafluorosilicate F_6Li_2Si	-9.27	-1.1	-6.6	1
Lithium Bis(fluorosulfonyl)imide (LiFSI) $F_2LiNO_4S_2$	-9.09	-1.68	-5.69	1
Lithium (Fluorosulfonyl)(trifluoro-methanesulfonyl)imide $CF_4LiNO_4S_2$	-9.07	-1.85	-5.72	1
Lithium 1,1,2,2,3,3-Hexafluoropropa-ne-1,3-disulfonimide $C_3F_6LiNO_4S_2$	-8.9	-1.53	-6.23	1
Lithium Bis(pentafluoroethanesulfonyl)imide $C_4F_{10}LiNO_4S_2$	-8.78	-1.61	-5.62	1
Lithium Bis(trifluoromethane)sulfonimide (LiTFSI) $C_2F_6LiNO_4S_2$	-8.76	-1.46	-6.25	1
Lithium Nonafluoro-1-butanesulfonate $C_4F_9LiO_3S$	-8.74	-1.62	-6.09	1
Lithium tetrachloroaluminate $LiAlCl_4$	-8.7	-1.55	-5.37	1
Lithium perchlorate $LiClO_4$	-8.66	-1.73	-6.23	1

Lithium trifluoromethanesulfonate (LiOTf) CF_3SO_3Li	-8.6	-1.56	-6.29	1
Lithium trifluoroacetate CF_3CO_2Li	-8.3	-1.46	-6.64	1
Lithium metaphosphate LiO_3P	-8.29	-1.92	-6.5	1
Lithium tetrachloropalladate (II) Li_2PdCl_4	-8.21	-1.71	-6.38	1
Lithium difluoro(oxalato)borate (LiDFOB) $LiBF_2(C_2O_4)$	-7.58	-1.82	-5.47	1
Lithium 5-methyl-1,3,4-thiadiazole-2-carboxylate $C_4H_3LiN_2O_2S$	-7.25	-1.85	-6.88	1
Lithium nitrite $LiNO_2$	-8.55	-0.65	-7.26	2
Lithium Carbonate Li_2CO_3	-8.39	-0.22	-8.08	2
Lithium Chloride LiCl	-8.26	-1.01	-6.92	2
Lithium iodoacetate $C_2H_2ILiO_2$	-8.04	-0.43	-7.14	2
Lithium Dodecyl Sulfate $C_{12}H_{25}LiO_4S$	-7.84	-1.28	-6.64	2
Lithium Bromide LiBr	-7.78	-1.08	-6.48	2
Lithium phosphate monobasic LiH_2PO_4	-7.68	-1.13	-7.04	2
O-Phospho-L-homoserine lithium salt $C_4H_{10}NO_6P$	-7.58	-1.43	-6.48	2
Dilithium sulphite Li_2SO_3	-7.41	-0.3	-7.65	2
Lithiumacrylate $C_3H_3LiO_2$	-7.26	-1.11	-7.4	2
DL-Lactic acid, lithium salt $C_3H_5O_3Li$	-7.2	-1.26	-7.02	2
Lithium L-lactate $C_3H_5LiO_3$	-7.2	-1.26	-7.02	2

5-cyclopropyl-1,3,4-oxadiazole-2-carboxylate lithium salt $C_6H_5LiN_2O_3$	-7.18	-1.46	-6.9	2
D-Altronic acid lithium salt $C_6H_{11}LiO_7$	-7.18	-1.36	-6.46	2
Lithium isobutyrate $C4H7LiO_2$	-7.16	-1.03	-7.44	2
Lithium acetate $C_2H_3LiO_2$	-7.15	-1.02	-7.51	2
Lithium 2-ethylhexanoate $C_8H_{15}LiO_2$	-7.14	-1.03	-7.36	2
Lithium 4-cyclohexanebutyrate $C_{10}H_{17}LiO_2$	-7.12	-1.02	-7.43	2
Lithium octanoate $C_8H_{15}LiO_2$	-7.12	-1.02	-7.44	2
Lithium DL-2-Hydroxybutyrate $C_4H_7LiO_3$	-7.11	-1.26	-6.99	2
D-(−)-Citramalic acid lithium salt $C_6H_5Li_3O_7$	-7.04	-0.98	-6.38	2
(R)-Mevalonic acid lithium salt $C_6H_{11}LiO_4$	-7.02	-1.21	-6.96	2
Lithium benzoate $C_7H_5LiO_2$	-6.91	-1.13	-7.27	2
Lithium Tartrate $C_4H_4Li_2O_6$	-6.78	-1.01	-7.11	2
Lithium oxalate $C_2O_4Li_2$	-6.73	-0.96	-7.45	2
Monolithium 4-methoxypyridine-3-boronate $C_6H_{13}BLiNO_6$	-6.49	-1.23	-7.64	2
Propofol β-D-Glucuronide Lithium Salt $C_{18}H_{25}LiO_7$	-6.49	-1.01	-6.32	2
Clavulanate Lithium $C_8H_8LiNO_5$	-6.48	-1.32	-6.71	2
Lithium p-toluenesulfinate $CH_3C_6H_4SO_2Li$	-6.28	-0.96	-7.31	2
Lithium salicylate $C_7H_5LiO_3$	-6.23	-1.04	-7.37	2
Lithium Bis(nonafluorobutanesulfonyl)imide $C_8F_{18}LiNO_4S_2$	-6.15	-0.79	-7.22	2

Lithium tetraphenylborate tris(1,2-dimethoxyethane) $C_{36}H_{50}BLiO_6$	-6.05	-1.13	-5.85	2
Lithium 3-morpholinopropanoate $C_7H_{12}LiNO_3$	-6.01	-1.1	-7.29	2
Lithium Acetylacetonate $C_5H_7LiO_2$	-5.99	-0.94	-8.02	2
2,2,6,6-Tetramethyl-3,5-heptane-dionato lithium $C_{11}H_{19}LiO_2$	-5.82	-0.8	-8.02	2
Cyclopentadienyllithium C_5H_5Li	-5.81	-1.01	-7.48	2
Ethylenediaminetetraacetic acid dilithium salt $C_{10}H_{14}Li_2N_2O_8$	-5.61	-0.98	-6.38	2
Lithium oxide Li_2O	-4.94	-0.16	-9.2	2
Lithium peroxide Li_2O_2	-4.73	-0.17	-8.29	2
Lithium nitride Li_3N	-3.68	-0.17	-9.04	2
Lithium hexafluoroarsenate(V) $LiAsF_6$	-11	-2.85	-5.83	3
Lithium bis(oxalate)borate (LiBOB) C_4BLiO_8	-8.51	-2.31	-6.09	3
Lithium bis(oxalato)borate C_4BLiO_8	-8.42	-2.85	-4.96	3
Li difluorophosphate $LiPO_2F_2$	-8.37	-2.04	-5.6	3
Lithium 4,5-dicyano-2-(trifluoro-methyl) imidazol-1-ide $C_6F_3LiN_4$	-7.32	-2.09	-5.46	3
Lithium Tetrakis(pentafluorophenyl) borate - Ethyl Ether Complex $C_{24}BF_{20}Li$	-7.24	-2.36	-4.82	3
Lithium metaborate $LiBO_2$	-7.23	-1.94	-6.15	3
Sulfopyruvic acid dilithium salt $C_3H_4Li_2O_6S$	-7.05	-2.03	-5.44	3

Lithium;2-oxo-2-(tetrafluoro-lambda 5-phosphanyl) oxyacetate $LiF_4C_2O_4P$	-7.02	-3.11	-4.78	3
Lithium [1,2,4] triazolo[4,3-a] pyrazine-3-carboxylate $C_6H_3LiN_4O_2$	-6.9	-2.08	-6.67	3
5-Sulfoisophthalic acid monolithium salt $C_8H_5LiO_7S$	-6.71	-1.53	-3.82	3
Lithium acetate dihydrate CH_3COOLi	-5.92	-2.33	-4.3	3
Phenyllithium solution C_6H_5Li	-3.49	-3.28	-7.13	3
Lithium iodate $LiIO_3$	-9.4	-0.26	-10.42	4
Lithium 5-bromopyridine-2-carboxylate $C_6H_3BrLiNO$	-7.1	-1.71	-7.09	4
Dihydroxyacetone phosphate dilithium salt $C_3H_5Li_2O_6P$	-7	-1.96	-7.73	4
Lithium 3-fluoropyridine-2-carboxylate $C_6H_3FLiNO_2$	-7	-1.64	-7.03	4
DL-4-Hydroxy-2-ketoglutarate Dilithium Salt $C_5H_4Li_2O_6$	-6.58	-1.58	-7.6	4
Lithium acetoacetate $C_4H_5LiO_3$	-6.54	-1.8	-7.17	4
Adenosine 5′-O-thiomonophosphate dilithium salt $C_{10}H_{12}N_5O_6PSLi_2$	-6.48	-1.38	-6.83	4
Lithium Phenyl(2,4,6-trimethyl-benzoyl) phosphinate $C_{16}H_{16}LiO_3P$	-6.4	-1.61	-6.93	4

6-Hydroxy Chlorzoxazone β-D-Glucuronide Lithium Salt $C_{13}H_{11}ClLiO_9$	-6.31	-1.46	-6.52	4
Lithium trimethylsilanolate C_3H_9LiOSi	-6.29	-1.43	-7.48	4
Lithium phosphate Li_3PO_4	-6.12	-1.25	-7.74	4
5-Methylpyridine-2-boronic acid, mono-lithium salt $C_6H_7BLiNO_2$	-5.88	-1.67	-6.99	4
Profoxydim lithium salt $C_{24}H_{31}ClLiNO_4S$	-5.64	-1.32	-7.43	4
Lithium bis(trimethylsilyl)amide $C_6H_{18}LiNSi_2$	-5.59	-1.31	-6.89	4
(8-Quinolinolato) lithium C_9H_6LiNO	-5	-1.68	-7.66	4
Lithium 2-(2', 2''-bipyridine-6'-yl) phenolate $C_{16}H_{11}LiN_2O$	-4.98	-2.14	-7.61	4
Methyllithium solution CH_3Li	-4.84	-1.39	-7.64	4
Isobutyllithium C_4H_9Li	-4.59	-1.45	-7.42	4
Hexyllithium $C_6H_{13}Li$	-4.53	-1.47	-7.45	4
sec-Butyllithium solution C_4H_9Li	-4.53	-1.47	-7.46	4
Ethyllithium solution CH_3CH_2Li	-4.45	-1.45	-7.6	4
Lithium sulfide Li_2S	-4.32	-1.08	-7.47	4
tert-Butyllithium C_4H_9Li	-4.22	-1.61	-7.12	4
Lithium diisopropylamide $C_6H_{14}LiN$	-4.17	-1.27	-7.53	4
Lithium dicyclohexylamide $(C_6H_{11})_2NLi$	-4.1	-1.24	-7.51	4
Lithium diethylamide $C_4H_{12}LiN$	-4.07	-1.28	-7.58	4
Lithium dimethylamide C_2H_6LiN	-3.97	-1.35	-7.66	4

Supplementary Table 3|Summary of LE, SDE, and UDE electrolytes.

	Abbreviation	Electrolyte composition
LE	LE1	1 M $LiPF_6$ EC/EMC (1:1:1:1:1, vol.)
	LE2	1 M $LiPF_6$ FEC/FEMC (1:1:1:1:1, vol.)
SDE	SDE1	1 M $LiPF_6$ FEC/FEMC/DFEC/1FEMC/TTE (1:1:1:1:1, vol.)
	SDE2	1 M $LiBF_4$ FEC/FEMC/DFEC/1FEMC/TTE (1:1:1:1:1, vol.)
	SDE3	0.2 M LiDFOB FEC/FEMC/DFEC/1FEMC/TTE (1:1:1:1:1, vol.)
	SDE4	1 M LiTFSI FEC/FEMC/DFEC/1FEMC/TTE (1:1:1:1:1, vol.)
	SDE5	1 M LiOTf FEC/FEMC/DFEC/1FEMC/TTE (1:1:1:1:1, vol.)
UDE	UDE1	0.2 M $LiPF_6$/0.2 M $LiBF_4$/0.2 M LiDFOB/ 0.2 M LiTFSI/0.2 M LiOTf FEC/FEMC/DFEC/1FEMC/TTE (1:1:1:1:1, vol.)
	UDE2	0.2 M $LiPF_6$/0.2 M $LiBF_4$/0.2 M LiDFOB/ 0.2 M LiTFSI/0.2 M lithium bis(pentafluoroethanesulfonyl)imide FEC/FEMC/TFPC/1FEMC/HFDEC (1:1:1:1:1, vol.)
	UDE3	0.2 M $LiPF_6$/0.2 M $LiBF_4$/0.2 M LiDFOB/ 0.2 M LiFSI/0.2 M lithium nonafluoro-1-butanesulfonate FEC/FEMC/DFEC/TFPC/TTE (1:1:1:1:1, vol.)

Supplementary Table 4|Summary of simulated models for LE, SDE, and UDE electrolytes.

Abbreviation	Electrolyte composition
LE1	50 $LiPF_6$, 375 EC, and 240 EMC
LE2	50 $LiPF_6$, 343 FEC, and 208 FEMC
SDE1	50 $LiPF_6$, 137 FEC, 83 FEMC, 123 DFEC, 98 1FEMC, and 66 TTE
SDE2	50 $LiBF_4$, 137 FEC, 83 FEMC, 123 DFEC, 98 1FEMC, and 66 TTE
SDE3	10 LiDFOB, 137 FEC, 83 FEMC, 123 DFEC, 98 1FEMC, and 66 TTE
SDE4	50 LiTFSI, 137 FEC, 83 FEMC, 123 DFEC, 98 1FEMC, and 66 TTE
SDE5	50 LiOTf, 137 FEC, 83 FEMC, 123 DFEC, 98 1FEMC, and 66 TTE
UDE1	10 $LiPF_6$, 10 $LiBF_4$, 10 LiDFOB, 10 LiTFSI, 10 LiOTf, 137 FEC, 83 FEMC, 123 DFEC, 98 1FEMC, and 66 TTE

Supplementary Table 5|Summary of simulated models for LE, SDE, and UDE electrolytes after Anneal.

Abbreviation	Electrolyte composition	Cell size (Å)
LE1	50 $LiPF_6$, 375 EC, and 240 EMC	47.45
LE2	50 $LiPF_6$, 343 FEC, and 208 EMC	47.06
SDE1	50 $LiPF_6$, 137 FEC, 83 FEMC, 123 DFEC, 98 1FEMC, and 66 TTE	46.08
SDE2	50 $LiBF_4$, 137 FEC, 83 FEMC, 123 DFEC, 98 1FEMC, and 66 TTE	45.68
SDE3	50 LiDFOB, 137 FEC, 83 FEMC, 123 DFEC, 98 1FEMC, and 66 TTE)	45.34
SDE4	50 LiTFSI, 137 FEC, 83 FEMC, 123 DFEC, 98 1FEMC, and 66 TTE	46.74
SDE5	50 LiOTf, 137 FEC, 83 FEMC, 123 DFEC, 98 1FEMC, and 66 TTE	46.07
UDE1	10 $LiPF_6$, 10 $LiBF_4$, 10 LiDFOB, 10 LiTFSI, 10 LiOTf, 137 FEC, 83 FEMC, 123 DFEC, 98 1FEMC, and 66 TTE	46.16

Supplementary Table 6|Summary of simulated models for LE, SDE, and UDE electrolytes after NVT at different temperatures.

Abbreviation	253K		298K		318K	
	Cell size (Å)	Density (g cm^{-3})	Cell size (Å)	Density (g cm^{-3})	Cell size (Å)	Density (g cm^{-3})
LE1	1.316	43.79	1.272	44.28	1.268	44.33
LE2	1.589	43.14	1.522	43.84	1.497	44.01
SDE1	1.609	43.14	1.549	43.69	1.535	43.82
SDE2	1.579	42.86	1.516	43.45	1.485	43.75
SDE3	1.555	42.45	1.497	43.99	1.469	43.26
SDE4	1.659	43.98	1.601	44.42	1.560	44.81
SDE5	1.603	43.23	1.541	43.80	1.503	44.17
UDE1	1.604	43.32	1.547	43.79	1.528	44.03

Supplementary Table 7|The specifications of NCM811||Li pouch cell (510.1 Wh kg^{-1} in 1.9 Ah)

Cell component	Specification	Parameters
Anode (Li foil)	Thickness (μm)	50.0
Electrolyte (UDE1, SDE1, LE1)	Electrolyte/Capacity (g Ah^{-1})	1.6
Separator (LATP coated PP)	Thickness (μm)	17.0
Cathode (4.45V-NCM 811)	Active material mass loading (mg cm^{-2}, each side)	31.8
	Active material ratio	0.96
	Al current collector (μm)	9.0
Package (Al-plastic film)	Size (mm × mm × mm)	42×30×5.9
Full cell	Discharge capacity (Ah)	1.8 (0.5C)
	Specific energy density (Wh kg^{-1})	510.1 (0.5C)
	Total weight (g)	14.03

Supplementary Table 8|The specifications of LCO||Li pouch cell (519.3 Wh kg^{-1} in 1.8 Ah)

Cell component	Specification	Parameters
Anode (Li foil)	Thickness (μm)	50.0
Electrolyte (UDE1, SDE1, LE1)	Electrolyte/Capacity (g Ah^{-1})	1.5
Separator (LATP coated PP)	Thickness (μm)	17.0
Cathode (4.6 V-LCO)	Active material mass loading (mg cm^{-2}, each side)	31.8
	Active material ratio	0.96
	Al current collector (μm)	12 .0
Package (Al-plastic film)	Size (mm × mm × mm)	42×30×5.4
Full cell	Discharge capacity (Ah)	1.8 (0.5C)
	Specific energy density (Wh kg^{-1})	519.3 (0.5C)
	Total weight (g)	14.01

Supplementary Table 9|The specifications of NCM811||Li pouch battery (554.8 Wh kg^{-1} in 6.9 Ah)

Cell component	Specification	Parameters
Anode (Li foil)	Thickness (μm)	50.0
Electrolyte (UDE1, SDE1)	Electrolyte/Capacity (g Ah^{-1})	1.2
Separator (LATP coated PP)	Thickness (μm)	17.0
Cathode (4.45 V-NCM811)	Active material mass loading (mg cm^{-2}, each side)	31.8
	Active material ratio	0.96
	Al current collector (μm)	12.0
Package (Al-plastic film)	Size (mm × mm × mm)	90×50×5.4
Full cell	Discharge capacity (Ah)	6.9 (0.2C)
	Specific energy density (Wh kg^{-1})	554.8 (0.2C)
	Total weight (g)	47.06

Supplementary Table 10|The specifications of NCM811||Li pouch cell (565.8 Wh kg^{-1} in 23.2 Ah)

Cell component	Specification	Parameters
Anode (Li foil)	Thickness (μm)	50.0
Electrolyte (UDE1)	Electrolyte/Capacity (g Ah^{-1})	1.2
Separator (LATP coated PP)	Thickness (μm)	17.0
Cathode (4.45 V-NCM811)	Active material mass loading (mg cm^{-2}, each side)	31.8
	Active material ratio	0.96
	Al current collector (μm)	12.0
Package (Al-plastic film)	Size (mm × mm × mm)	185×112×3.8
Full cell	Discharge capacity (Ah)	23.2 (0.1C)
	Specific energy density (Wh kg^{-1})	565.8 (0.2C)
	Total weight (g)	155.6

Supplementary Table 11|The specifications of Ni90||Li pouch cell (604.2 Wh kg^{-1} in 5.5 Ah)

Cell component	Specification	Parameters
Anode (Li foil)	Thickness (μm)	50.0
Electrolyte (UDE1)	Electrolyte/Capacity (g Ah^{-1})	1.0
Separator (Al_2O_3 coated PE)	Thickness (μm)	5.0
Cathode (4.3 V-Ni90)	Active material mass loading (mg cm^{-2}, each side)	35.7
	Active material ratio	0.96
	Al current collector (μm)	9.0
Package (Al-plastic film)	Size (mm × mm × mm)	90× 50×5.1
Full cell	Discharge capacity (Ah)	5.5 (0.2C)
	Specific energy (Wh kg^{-1})	604.2 (0.2C)
	Total weight (g)	34.93

Supplementary Table 12|The specifications of Ni90||Li pouch cell (618.2 Wh kg^{-1} in 5.2 Ah)

Cell component	Specification	Parameters
Anode (Li foil)	Thickness (μm)	50.0
Electrolyte (UDE1)	Electrolyte/Capacity (g Ah^{-1})	0.9
Separator (Al_2O_3 coated PE)	Thickness (μm)	5.0
Cathode (4.3 V-Ni90)	Active material mass loading (mg cm^{-2}, each side)	41.3
	Active material ratio	0.96
	Al current collector (μm)	9.0
Package (Al-plastic film)	Size (mm × mm × mm)	90× 50×4.8
Full cell	Discharge capacity (Ah)	5.2 (0.2C)
	Specific energy (Wh kg^{-1})	618.2 (0.2C)
	Total weight (g)	32.09

Supplementary Table 13|The performance comparisons of Ah-level Li-metal pouch cells (energy density over 300 Wh kg^{-1}) in recent reports and this work.

Capacity (Ah)	Energy density (Wh kg^{-1})	Cycle number	References
0.42	320	120	Ref 1
0.99	354	200	Ref 2
1.4	340	140	Ref 3
2.1	403	100	Ref 4
2.5	325	200	Ref 5
4.4	381	120	Ref 6
5.1	418.7	70	Ref 7
5.3	440	130	Ref 8
10	406	65	Ref 9
1.9	**510.1**	**300**	**This work**
1.8	**519.3**	**100**	
6.9	**554.8**	**90**	
23.2	**565.8**	**50**	
5.5	**604.2**	**100**	
5.2	**618.2**	**90**	

Supplementary Table 14|The specifications of the 3.9 KWh NCM811||Li battery pack.

Pack component	Specification	Parameters
Unit cell	Type	NCM811||Li
	Discharge capacity (Ah)	~22
	Weight (g)	~146
Protection shell	Type	Aluminum alloy
	Weight (g)	410
Cushioning material	Type	Foam material
	Weight (g)	240
Tie rod	Type	Titanium alloy
	Weight (g)	310
Battery management system	Weight (g)	105
Others	Type	Insulation tape, connection lines, et al
	Weight (g)	47
Circuit design	series-parallel circuit	24(series connection)×2 (parallel connection)
Full module	Total weight (g)	8120
	Total voltage (V)	104
	Discharge capacity (Ah)	42.6
	Specific energy (Wh kg^{-1})	480.7
	Total energy (Wh)	3904

Supplementary references

1. Zhang, S. et al. Oscillatory solvation chemistry for a 500 Wh kg^{-1} Li-metal pouch cell. *Nat. Energy* **9**, 1285–1296 (2024).
2. Chang, Z., Yang, H., Pan, A., He, P., & Zhou, H. *Nat. Commun*. **13**, 6788 (2022).
3. Huang, Y.et al. Eco-friendly electrolytes via a robust bond design for high-energy Li metal batteries. *Energy Environ. Sci*. **15**, 4349-4361 (2022).
4. Liu, Z., Guo, D., Fan, W., Xu, F., & Yao, X. Expansion-tolerant lithium anode with built-in LiF-rich interface for stable 400 Wh kg^{-1} lithium metal pouch cells. *ACS Mater. Lett.* **4**, 1516-1522 (2022).
5. Gao, Y. et al. Effect of the supergravity on the formation and cycle life of non-aqueous lithium metal batteries. *Nat Commun.* 13, 5 (2022).
6. Yang, B. et al. High-safety lithium metal pouch cells for extreme abuse conditions by implementing flame-retardant perfluorinated gel polymer electrolytes. *Energy Storage Mater*. **65**, 103124 (2024).
7. Zhao, P. Constructing self-adapting electrostatic interface on lithium metal anode for stable 400 Wh kg^{-1} pouch cells. *Adv. Energy Mater*. **12**, 2200568 (2022).
8. Zhang, Q. et al. Homogeneous and mechanically stable solid-electrolyte interphase enabled by trioxane-modulated electrolytes for lithium metal batteries. *Nat. Energy **8***, 725-735 (2023).
9. Zhang, K. et al. A High-Performance Lithium Metal Battery with Ion-Selective Nanofluidic Transport in a Conjugated Microporous Polymer Protective Layer. *Adv. Mater*. **33**, 2006323 (2021).